ATMOSPHERIC DENSITIES FROM EXPLORER 17 DENSITY GAUGES AND A COMPARISON WITH SATELLITE DRAG DATA*

GEORGE NEWTON, RICHARD HOROWITZ AND WOLFGANG PRIESTER†

The purpose of this letter is to present the initial atmospheric densities directly measured by the ionization gages on the Explorer 17 satellite. The satellite has been described [*Horowitz*, 1963] and the gauges and their response to the atmosphere have also been reported [*Newton et al.*, 1963]. The data presented in this letter were obtained with two types of ionization vacuum gauges, the hot-filament thermionic type (Bayard-Alpert) and the magnetron type (Redhead). The absolute accuracy of these data is believed to be ±35 percent and the repeatability is ±20 percent. A more complete discussion of the experiment will be included in a paper now in preparation [*Newton et al.*, 1964].

The density data from 47 operations of the satellite in the altitude range 255 to 330 km for local times between 0700 and 2100 hours are plotted as a function of altitude in Figure 1. These data were recorded by the five northern midlatitude minitrack stations:

Blossom Point, Md.
Grand Forks, Minn.
Mojave, Calif.
St. Johns, Newfoundland
Winkfield, England

At the times the measurements were made, the daily planetary geomagnetic index (A_p) was between 0 and 50, and the 10.7-cm solar index ($F_{10.7}$) was between 70 and 100×10^{-22} w/m^2 cps. It is seen from Figure 1 that there is considerable variation in the atmospheric density at a given altitude (that is, greater than a factor of 3 at the altitude of 280 km) which is due in part to local time, geomagnetic activity, and solar activity effects.

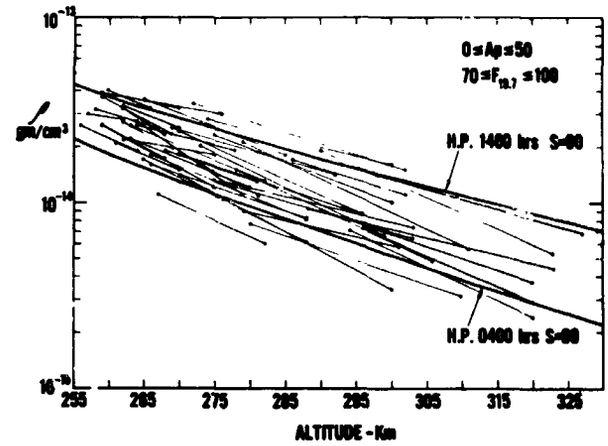

FIGURE 1.—Atmospheric density versus altitude measured by the Explorer 17 density gauges during 47 operations of the satellite. The densities were measured for times between 0700 and 2100 hours, with A_p varying between 0 and 50 and with $F_{10.7}$ varying between 70 and 100×10^{-22} w/m^2 cps.

To compare the directly measured densities with densities inferred from satellite drag, it is desirable to reduce the data to geomagnetically quiet conditions. In this regard, consider Figure 2, which shows $\Delta \log \rho$, the logarithm to the base 10 of the ratio of the measured density to the Harris and Priester model density selected for the appropriate time and altitude, plotted versus the daily geomagnetic index (A_p). These points represent 120 density-altitude profiles for altitudes between 255 and 600 km and most local times; the data were recorded over the same five minitrack stations as were the data in Figure 1. The darkened symbols represent an average of two or more

*Published in the *Journal of Geophysical Research*, 69(21):4690–4692, November 1, 1964.

†Goddard Space Flight Center; on leave from Bonn University.

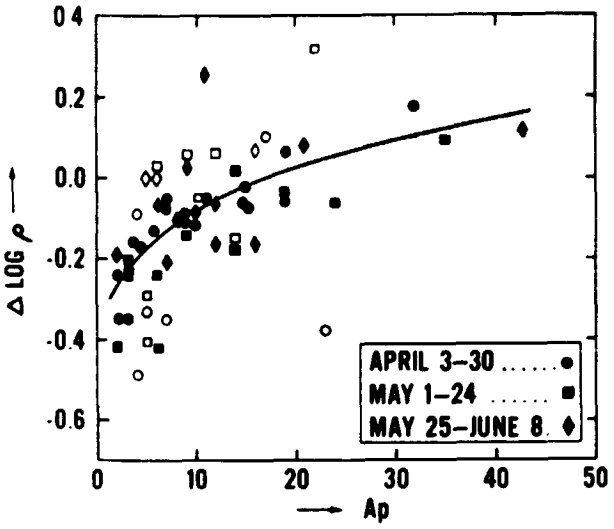

FIGURE 2.—Daily average of the logarithms of the ratios of the gauge measured density to the Harris and Priester model density, plotted against daily geomagnetic A_p index. Solid symbols represent averages of measurements obtained from two or more passes of the satellite over the telemetry stations. Open symbols represent single passes. The data have been adjusted to correspond to $F_{10.7}=83$. The semiannual variation of the atmospheric density has been accounted for in an approximate way by decreasing the model densities by 18% for May and June 1963.

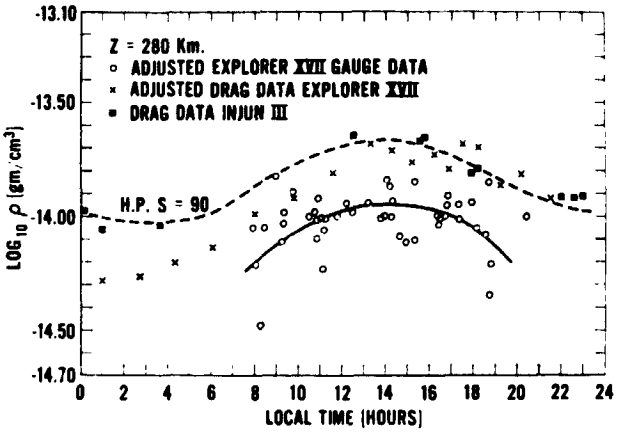

FIGURE 3.—Logarithms of densities normalized to an altitude of 280 km versus local time. Injun 3 data are selected for geomagnetically quiet conditions. Explorer 17 data are adjusted to $A_p=2$ using relation shown in Figure 2 and for an $F_{10.7}$ corresponding to 83.

passes within one day and the light symbols represent one pass. The passes have been individually corrected to an $F_{10.7}$ of 83 using *Roemer's* [1963] formula. The semiannual variation of the atmospheric density has been accounted for in an approximate way by decreasing the model densities by 18 percent for May and June 1963. A visual average of the data shows (*a*) that the relation between Δ log ρ and A_p is nonlinear, the steepest slope being applicable to the smaller A_p values, and (*b*) that the atmospheric density values are more sensitive to geomagnetic disturbances than has previously been reported. Very recently, *Jacchia and Slowey* [1964*a*] found independently that for near-quiet geomagnetic conditions the reaction of the atmosphere to variations in A_p is considerably larger than that expected on the basis of their previous analyses.

Figure 3 shows the logarithm to the base 10 of the gauge densities at the average time and altitude of the pass plotted versus local time and normalized to 280 km using the Harris and Priester model for $S=90$ as a differential altitude transformer. Shown for comparison are the densities obtained from drag observations of Injun 3 [*Jacchia and Slowey*, 1964*b*] and Explorer 17 [*Bryant*, 1964], and the Harris and Priester model with $S=90$. The drag data have also been normalized to the 280-km altitude.

The Injun 3 drag data, indicated by squares, were selected for quiet geomagnetic conditions ($A_p\pm2$) for the time interval of February 18 through June 30, 1963, when the latitude of the satellite varied between $-40°$ and $+60°$. The Explorer 17 drag data, indicated by crosses, correspond to the time interval from April 3 to July 6, 1963, when the satellite perigee was between $+58°$ and $-20°$.

The relation shown in Figure 2 has been used to adjust both the Explorer 17 drag-determined and gauge-measured densities to geomagnetically quiet conditions ($A_p=2$). The Explorer 17 densities also have been normalized to a 10.7-cm solar index of 83, a small adjustment compared to those associated with the A_p. The A_p adjustment resulted in: (*a*) a decrease of approximately a factor of 2 in the apparent scatter between the gauge-measured density values, (*b*) a lowering of the average of the gauge-measured densities by a factor of 0.7, and (*c*) a lowering of Bryant's drag densities by approximately 60 percent.

It is seen in Figure 3 that the atmospheric densities determined by satellite drag techniques appear to be systematically higher by a factor of 2 than the adjusted gauge densities. This difference is greater than the combined uncertainties

assigned to the separate sets of data and would seem to be due to a systematic error in one or both of the measurements. While the difference is not regarded as a serious discrepancy between the two techniques, it is large enough to require a re-examination of the measurements made by each.

A more detailed presentation of the atmospheric density data from these five minitrack stations and their geophysical interpretation is in preparation [*Newton et al.*, 1964]. The presentation will include (1) data of considerably greater altitude and local-time coverage and (2) density scale-height computations. In addition, data from the other eight minitrack (perigee 255 km, initial apogee 920 km, 58° inclination) are currently being analyzed and will be reported.

ACKNOWLEDGMENTS

We wish to thank Mr. Nelson W. Spencer, Goddard Space Flight Center, for helpful discussions in the preparation of this letter.

One of us (W. Priester) is grateful to the National Academy of Sciences—National Research Council for a Senior Research Associateship.

REFERENCES

BRYANT, R., Densities obtained from drag on the Explorer 17 satellite, *J. Geophys. Res.*, *69*, 1423–1425, 1964.

HARRIS, I., and W. PRIESTER, Heating of the upper atmosphere, *Space Res.*, *3*, 53–75, 1963.

HOROWITZ, R., S-6, an aeronomy satellite, *Advan. Astronautical Sci.*, *12*, Western Periodicals Company, North Hollywood, California, 1963.

JACCHIA, L. G., and J. SLOWEY, Temperature variations in the upper atmosphere during geomagnetically quiet intervals, *Smithsonian Inst. Astrophys. Obs. Rept. 152*, June 1964*a*.

JACCHIA, L. G., and J. SLOWEY, Atmospheric heating of the auroral zones: A preliminary analysis of atmospheric drag of the Injun 3 satellite, *J. Geophys. Res.*, *69*, 905–910, 1964*b* (*SAO Spec. Rept. 136*, September 1963).

NEWTON, G. P., R. HOROWITZ, and W. PRIESTER, Explorer 17 pressure gauge experimental data and interpretation, in preparation, 1964.

NEWTON, G. P., D. T. PELZ, G. E. MILLER, and R. HOROWITZ, Response of modified Redhead magnetron and Bayard-Alpert vacuum gauges aboard Explorer 17, *Transactions of the Tenth National Vacuum Symposium*, edited by George H. Bancroft, pp. 208–212, The Macmillan Company, New York, 1963.

ROEMER, M., Die Dichte der Hochatmosphäre und Ihre Variationen während der Phase abklingender Sonnenaktivitat, 1958–1962, *Veroeffentl. Univ. Sternwarte Bonn*, *68*, 1963.

STRATOSPHERIC TEMPERATURE PATTERNS BASED ON RADIOMETRIC MEASUREMENTS FROM THE TIROS VII SATELLITE*

W. NORDBERG, W. R. BANDEEN, G. WARNECKE AND V. KUNDE

The TIROS VII meteorological satellite carried a sensor to map the emitted terrestrial radiation in the 15 micron carbon dioxide band. The spectral response of the sensor ranged from 14.8 to 15.5 microns. The radiation observed by the satellite is a function of the temperatures of the atmosphere varying along the optical path. Atmospheric layers at various altitudes contribute to the observed radiation in varying amounts. More than 96 percent of this contribution stems from altitudes above 10 km and more than 60 percent from a layer ranging in altitude from 18 to 35 km; thus, the radiation measurements were interpreted in terms of average temperatures of a major portion of the stratosphere.

Temperature patterns were analyzed from June 1963 to March 1964. The measurements demonstrate on a global scale, the varying patterns of stratospheric temperatures and circulation. Smooth temperature gradients were found to coincide closely with latitudinal circles on both summer hemispheres. Temperatures increased at high latitudes toward the summer pole (250° K) and rapidly decreased toward the winter pole (200° K).

A fairly uniform region with temperatures generally around 230° K extended between 25° latitude of the summer hemisphere and 40° latitude of the winter hemisphere during solstices. During both equinoxes, the large latitudinal temperature gradients at high latitudes disappeared and differences of about 10–15° K existed with latitudes as well as with longitude. Winter temperature patterns in both hemispheres exhibit strong temperature gradients between the pole and 40°, but a completely uniform pattern never existed in either winter hemisphere. A warm area over the Indian Ocean, though initially small, seemed to play a similar role in the southern winter as the Aleutian warm center during the northern winter. The morphology of a stratospheric warming which occurred over southwestern Asia and penetrated to Europe immediately after the tropical belt had cooled by about 10° K was observed.

I. INTRODUCTION

A radiometer aboard the TIROS VII satellite measured infrared radiation emitted mainly by carbon dioxide in the earth's atmosphere at wavelengths ranging from 14.8 to 15.5 microns. The instrument in this measurement was very similar to the 5 channel radiometers flown on previous TIROS satellites and described by Bandeen, et al. (Reference 1), except that one of the optical channels was modified to have a spectral response as shown in Figure 1a. The initial objective of radiation measurements in this region of the spectrum was to study the characteristics of the earth's horizon as described by Hanel, et al. (Reference 2) and later reported by Bandeen, et al. (Reference 3). Now, with continuous observations over a period of more than six months, covering daily the global zone from 65° N to 65° S, it is possible to use the radiation measurements to describe a number of interesting features of the atmosphere. It will be shown that most of the radiation reaching the satellite in this spectral region is emitted within a defined altitude interval in the stratosphere whose average temperature can be derived from the observed radiation intensities. Quasi-global maps of these average temperatures for different seasons not only reflect the expected variations in the mean stratospheric temperatures, but also reveal the development and behavior of major synoptic systems in that region of the atmosphere. A complete description

*Published as *Goddard Space Flight Center Document X-651-64-115*, May 1964.

†On leave from Institut für Meteorologie und Geophysik der Freien Universität Berlin, Berlin, Germany, as National Academy of Sciences-National Research Council Research Associate with National Aeronautics and Space Administration.

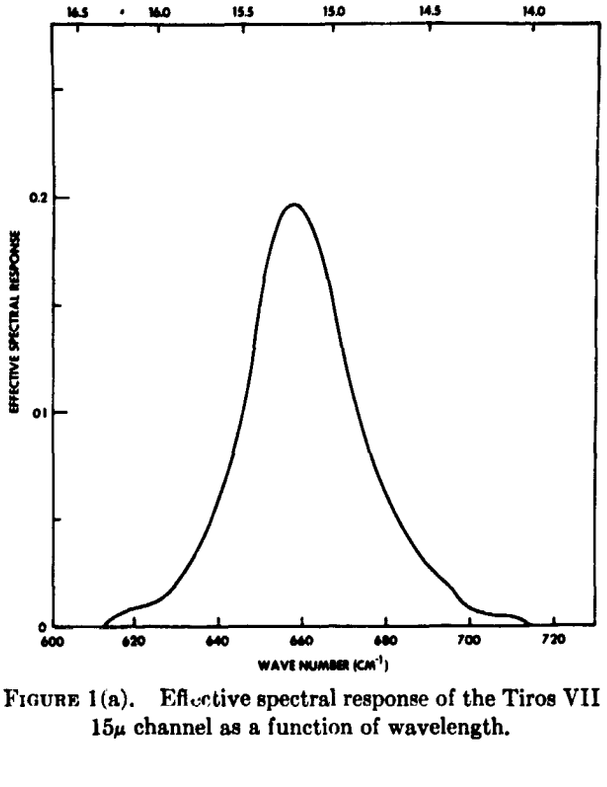

FIGURE 1(a). Effective spectral response of the Tiros VII 15μ channel as a function of wavelength.

of the 5 channel radiation experiment on TIROS VII as well as a critique and summary of all data resulting from this experiment will be contained in the TIROS VII Radiation Data Catalog and Users' Manual (Reference 4).

II. RELATION BETWEEN RADIATION AND STRATOSPHERIC TEMPERATURES

The spectral response of the instrument was chosen to coincide as closely as possible with the 15 micron absorption band of carbon dioxide. The radiance N from the earth and atmosphere measured by the radiometer whose spectral response function $\phi(\lambda)$ is shown in Figure 1a can be expressed as:

$$N=\frac{1}{\pi}\int_0^{\infty}\int_{\lambda=\lambda_1}^{\lambda_2}\phi(\lambda)B(\lambda, T)\frac{\partial\tau}{\partial s}(\rho, p, T, \lambda)d\lambda ds \qquad (1)$$

where

ρ = carbon dioxide density

B = Planck function

s = distance along radiation path

λ_1 and λ_2 = wavelengths between which $\phi\neq 0$

p = atmospheric pressure

T = atmospheric temperature

τ = atmospheric beam transmissivity

It is reasonable to assume that a constant ratio $r=0.000471$ exists between the densities ρ for carbon dioxide and ρ_{air} for air: $\rho=r\,\rho_{air}$. Furthermore, a number of typical distributions for temperature with height h for surface pressures of 1013.25 mb were chosen so that ρ_{air}, p and T could be expressed as functions of h where ρ_{air} and p were computed as a function of h from T by the hydrostatic equation. A relationship between s and h, $s=s(h)$, was established through the choice of several angles at which the satellite at approximately 635 km viewed the earth. The integration of (1) over λ was then performed for seven nadir angles, 0°, 29°, 40°, 47°, 52°, 55°, and 58°. The function $\tau(\lambda, h)$ was determined using, in principle, the method described by Hanel, et al. (Reference 2). That method is based on the general treatment by Elsasser (Reference 5) of the absorption within the 15 micron CO_2 band. Thus,

$$\int_{\lambda_1}^{\lambda_2}\phi(\lambda)B(h, \lambda)\frac{\partial\tau}{\partial s}(h, \lambda)\frac{\partial s}{\partial h}d\lambda=\Psi(h). \qquad (2)$$

Hence,
$$\bar{N}=\frac{1}{\pi}\int_0^{\infty}\Psi(h)dh. \qquad (3)$$

$\bar{N}$ was then computed for each of the assumed temperature profiles and for each nadir angle from (3). The assumed temperature distributions with height and the resulting distribution functions $\Psi(h)$ are shown in Figures 2a through 2c. In accordance with previous practices of reporting TIROS radiation measurements (References 4, 6–8) $\bar{N}$ may be expressed by the temperature T_{BB} of a blackbody whose radiant emittance $\bar{W}$ is given by:

$$\bar{W}=\int_{\lambda_1}^{\lambda_2}\phi(\lambda)B(T_{BB}, \lambda)d\lambda=\pi\bar{N} \qquad (4)$$

Indeed, since the radiometers were calibrated using such blackbodies at various temperatures, the measurement of T_{BB} may be considered as the

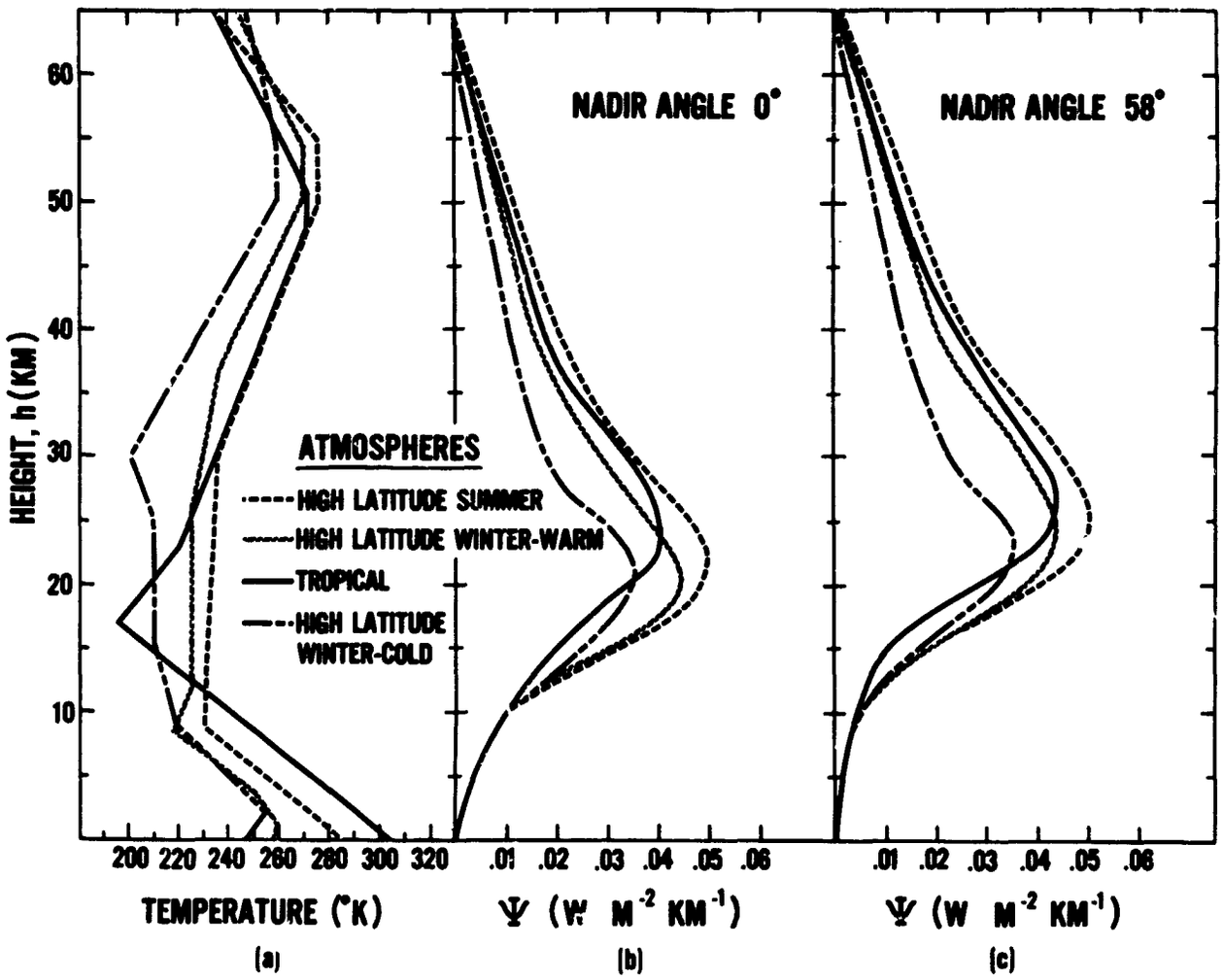

FIGURE 2(a).—Typical temperature profiles based on proposed supplements to the "U. S. Standard Atmosphere 1962" for 60° North summer, 60° North winter (warm and cold) and 15° North. The "warm" and "cold" temperature profiles for 60° N ("high latitude winter") can be considered typical at these latitudes depending on the state of the stratosphere in these regions. The supplements to the U. S. Standard Atmosphere 1962 are in the process of preparation by the U. S. Committee for Extension of the Standard Atmosphere and were summarized by Cole, et al. Reference 16).

FIGURE 2(b).—Weighting functions ψ (h), applying to the measured outgoing radiance $\bar{N}$; nadir angle = 0°

FIGURE 2(c).—Weighting functions ψ (h), applying to the measured outgoing radiance $\bar{N}$; nadir angle = 58°.

primary quantity while N requires a derivation by means of equation (4). The values of T_{BB} corresponding to the temperature profiles of Figure 2a are summarized in Table I.

The radiation measurement expressed by T_{BB} thus represents a mean temperature of the atmosphere in which the vertical temperature distribution is open to choice and where the temperature at each altitude must be given a different weight regarding its contribution to the measured mean. The weighting function is given by Ψ (h), and although Ψ (h) depends to a certain degree on the

TABLE I.—*Computed Mean Temperatures (T_{BB}) Expected to be Observed by 15 Micron Radiometer for Temperature profiles shown in Figures 2a at Nadir Angles of 0° and 58°.*

Nadir Angle	Tropical	High Lat. Summer	High Lat. Winter Cold	High Lat. Winter Warm
0°	227° K	238	213	229
58°	231	240	214	231

assumed vertical temperature profile, it may be seen that for most realistic temperature profiles at a nadir angle $\eta=0$ (Figure 2b), temperatures between 20 and 25 km are weighed most heavily with about 65 percent of the weight being concentrated in the region from 15 to 35 km and more than 96 percent of the weight lying at altitudes above 10 km. It may, also, be seen from Figure 2c that the maximum weight shifts to somewhat higher altitudes for a nadir angle of 58°. But, since this shift amounts to less than 5 km from $\eta=0$ to $\eta=58°$, it is not possible to make a precise quantitative determination of the variation of temperature with altitude from measurements of T_{BB} at various nadir angles. However, it will be shown in the section below that from such measurements one may infer qualitatively whether the temperature is increasing, decreasing, or constant with height over the altitude range where the Ψ functions reach their maxima. Furthermore, with a prudent and realistic choice of assumed vertical temperature profiles, such as shown in Figures 2a, one can easily determine from the T_{BB} measurements which one of these profiles represents the best fit qualitatively to actual conditions at a certain location on the globe and; more important, one may determine from continuous observations how the choices of such "best fits" vary with time. Thus, the maps of T_{BB} measurements plotted for the "quasi-global" (65° N to 65° S) zone for different times of the year, presented in Figures 3–12, enable the synoptic analysis of phenomena related to the temperature structure in the stratosphere between about 15 and 35 km. The occurrence of such events as explosive warmings, the establishment of the Aleutian anticyclone in winter, the onset of the seasonal circulation reversals and similar events may be categorized as such phenomena. Although the TIROS VII radiometer views the entire global zone from 65° N to 65° S during the course of 12 hours, data from only about 60 percent of the orbits during any one

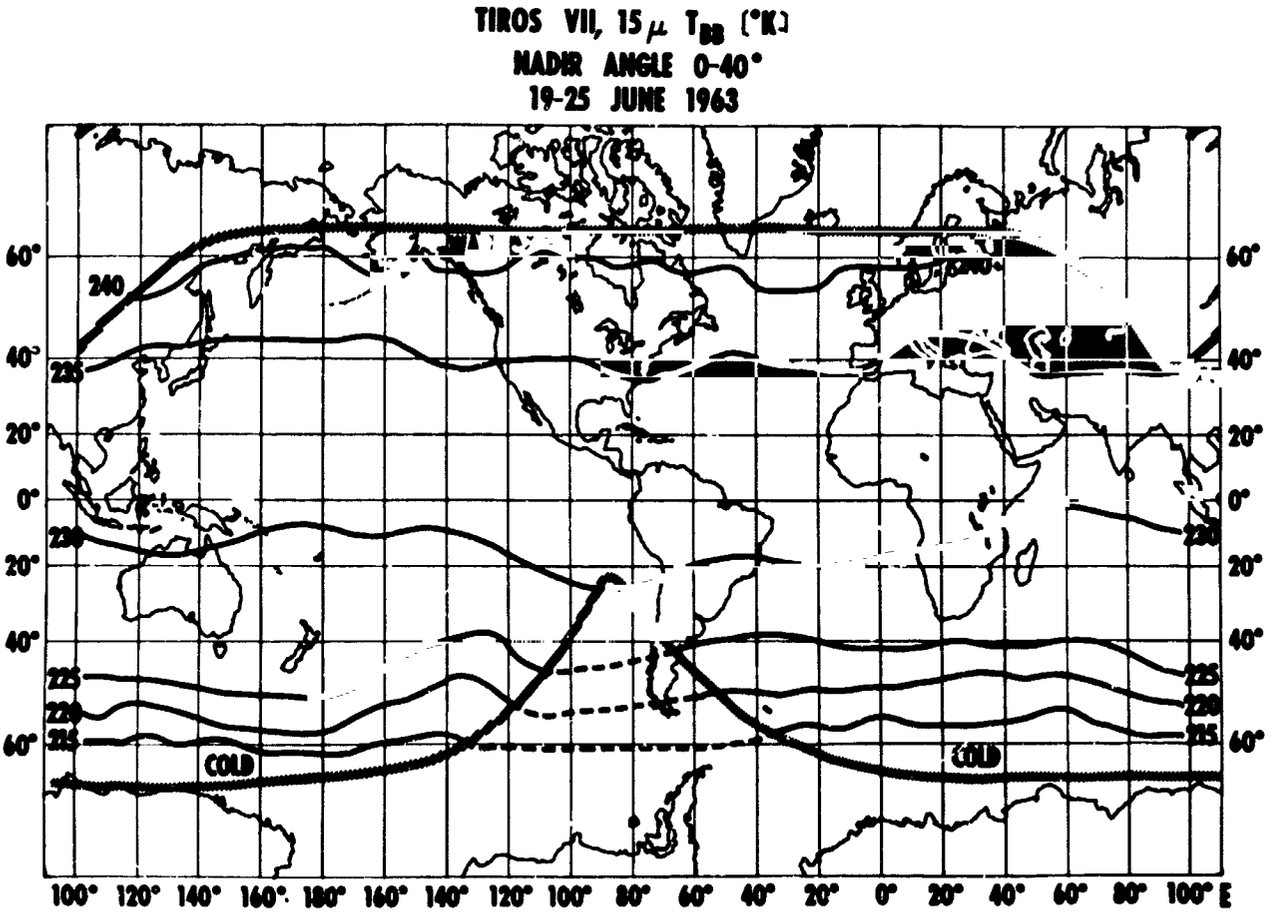

FIGURE 3(a).—Quasi-global map of 15μ equivalent blackbody temperatures averaged over the week 19–25 June 1963; nadir angle 0°–40°. Radiation data cannot be obtained outside the area enclosed by the dashed border.

day can be acquired because only stations within the United States are capable of receiving the data which are stored aboard the satellite for no longer than one orbital period. This causes two significant gaps in the data displayed in the maps, Figures 3–12. One such gap exists at 90° W just off the west coast of South America, the other is at 90° E over the central Soviet Union.

As will be stated in the TIROS VII Radiation Data Catalog and Users' Manual (Reference 4), the precision of each individual measurement is probably not much better than ±3°K. However, one may assume that the physical properties of the stratosphere remain generally constant for several days and are uniform over distances of less than 500 km. Since the field of view of the radiometer is about 5 degrees, covering an area of about 50×50 km on the surface of the earth for small nadir angles, and since in general measurements for the entire quasi-globe are obtained at least once every 24 hours, up to about 1000 measurements may result within one week within an area of about 500×500 km. Therefore, a precision of better than 1°K can be estimated for the temperature values shown in the maps, Figures 3–9 and 11–12, which were obtained by averaging measurements within each grid element (ranging from 5° latitude×5° longitude at the equator to 2.5° latitude×5° longitude at 60° latitude) over the period of one week.

Although the precision of the temperature measurement is greatly enhanced by reducing the random error in the averaging process, there are a number of systematic errors which must be considered. It has been attempted to reduce these errors by applying the appropriate corrections, but uncertainties still remain, causing the overall accuracy to be considerably poorer than the fraction of 1°K stated for the precision. Aside from correcting for an instrumental degradation which will be discussed later, a correction was applied to the data for an as yet unexplained deviation from

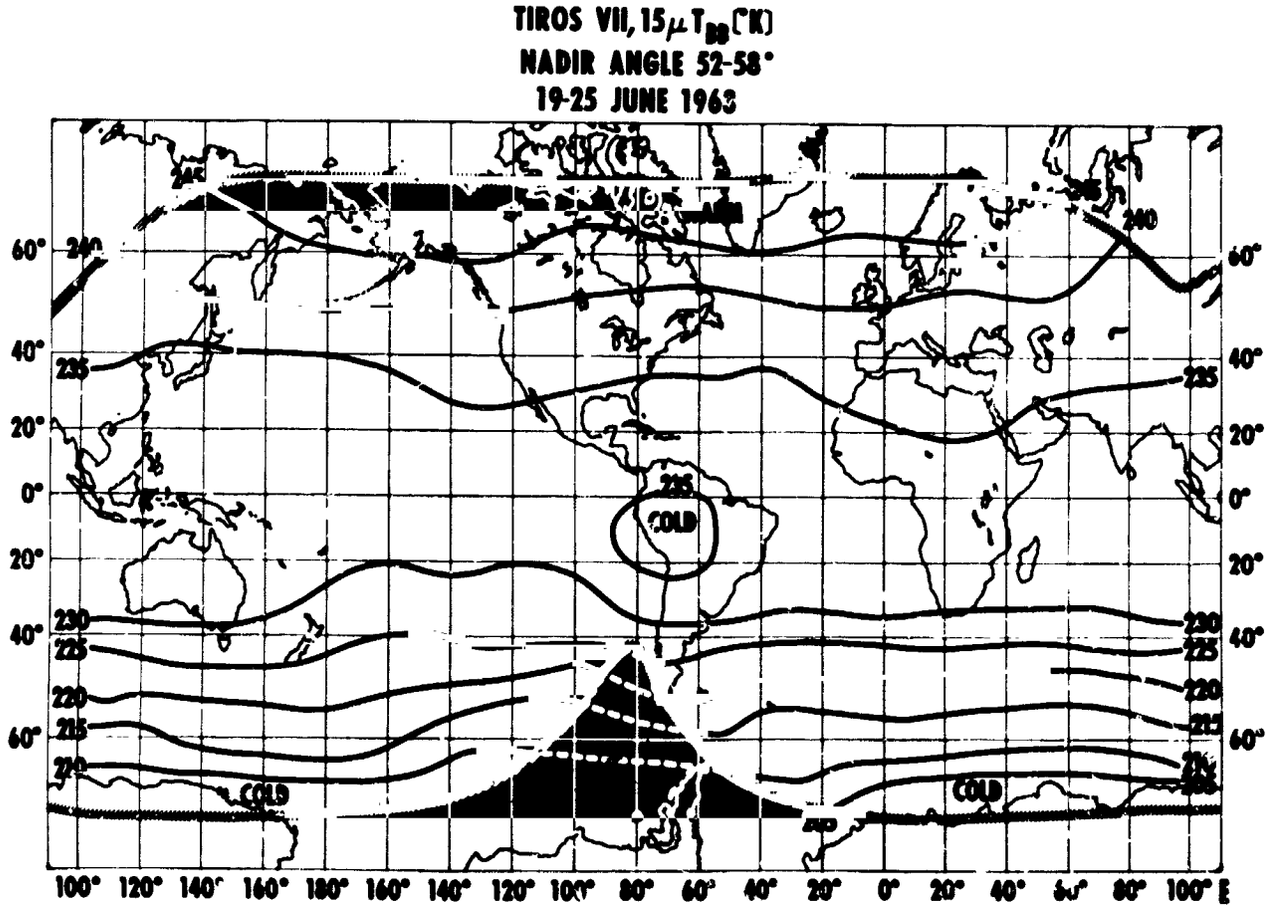

FIGURE 3(b).—Quasi-global map of 15μ equivalent blackbody temperatures averaged over the week 19–25 June 1963; nadir angle 52°–58°. Radiation data cannot be obtained outside the area enclosed by the dashed border.

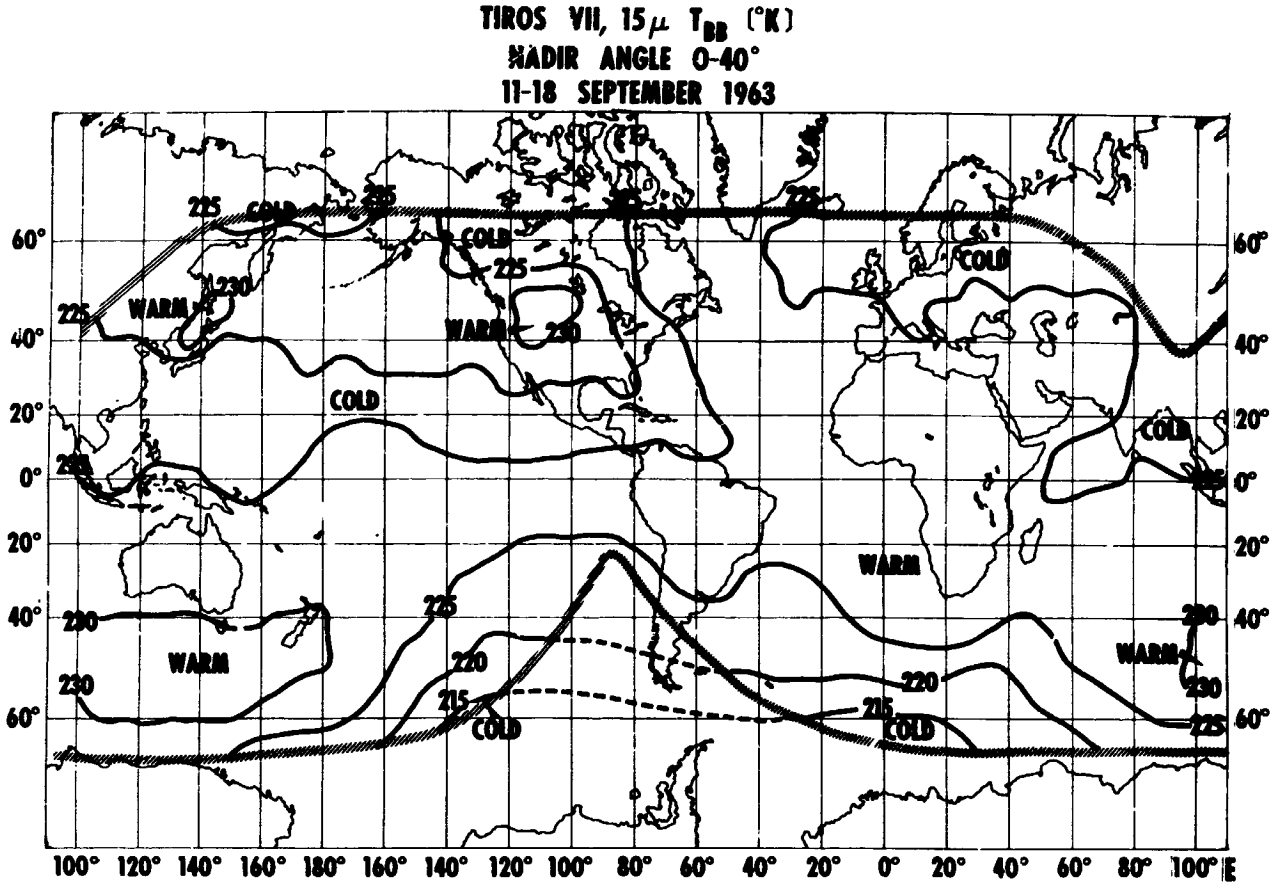

FIGURE 4.— Quasi-global map of 15μ equivalent blackbody temperatures averaged over the week 11–18 September 1963; nadir angle 0°–40°. Radiation data cannot be obtained outside the area enclosed by the dashed border.

the original preflight calibration. The radiometer, which alternatingly views the earth through one of two viewing ports showed that a consistently lower response on one of these viewing ports with respect to the other were apparently causing half of the measured temperatures to be too low and half to be too high. According to the preflight calibration, there should be no such difference. For lack of a better correction procedure, the difference between the temperatures measured through the two viewing ports over the same area at the same time were determined for all cases shown in the maps in Figures 3 through 12. Temperatures for the lower side were then corrected upward by half this difference, while those for the higher side were corrected downward by the same amount. Total differences were generally 5 to 8°K, so that the corrections were in the order of 2.5 to 4°K.

The maps were prepared from the magnetic tapes (FMRT's) containing all the TIROS VII radiation data (Reference 4) by an IBM 7094 computer and contour lines were drawn manually. This mapping procedure was the same as the one used in previously published similar maps (Reference 9).

III. ANALYSIS OF STRATOSPHERIC TEMPERATURES, JUNE 1963 TO MARCH 1964

A. Solstice June 1963

A typical temperature pattern at the start of the northern hemisphere summer and southern hemisphere winter for the quasi-globe is shown in Figure 3a. Stratospheric mean temperatures averaged over nadir angles between 0° and 40° and averaged over the week from 19 June to 25 June, the first week of TIROS VII, range from 240°K near 60° N to 215° near 60° S. The generally zonal structure of the temperature pattern, with isotherms running practically parallel with

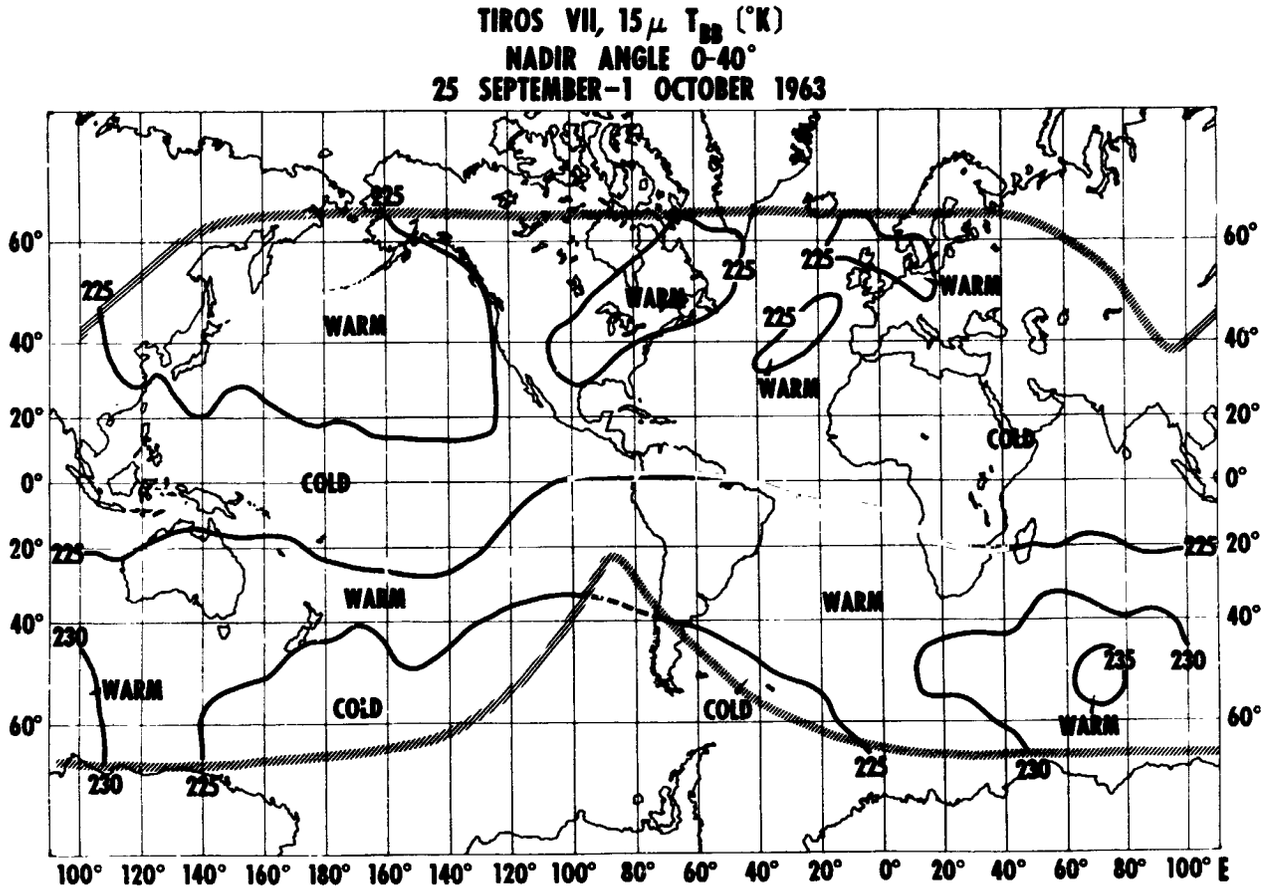

FIGURE 5.—Quasi-global map of 15μ equivalent blackbody temperatures averaged over the week 25 September–1 October 1963; nadir angle 0°–40°. Radiation data cannot be obtained outside the area enclosed by the dashed border.

latitude circles, confirms the established knowledge of the physics of the lower stratosphere; namely, the existence of a very strong cyclonic circulation system around a low pressure core centered near the winter pole. This low pressure is caused by the intense cooling of the stratosphere over the winter pole. Conversely, anticyclonic circulation prevails over the summer pole where solar heating causes a warm stratosphere resulting in a high pressure system. The predominantly zonal isotherms at high northern latitudes (summer) suggest that solar heating is primarily responsible for this pattern. At high southern latitudes (winter) however, there are slight but apparently significant disturbances in this zonal pattern. Isotherms over the South Pacific between 30° S and 60° S deviate from a perfect zonal course; they show a definite slope from the southwest to the northeast in that area. Temperatures increase rapidly from the winter pole toward the equator causing very steep temperature gradients with latitude in the winter hemisphere. A temperature of about 230°K is reached near 20° S. From there to the summer pole, the temperature increases gradually, and the gradients are not as steep as over the winter hemisphere. This is expected and it demonstrates clearly that the winter cyclone is considerably stronger than the summer anticyclone. The measured mean temperatures of 215°K near 60° S and of 240°K near 60° N agree reasonably well with the computed values of 213° and 238°K respectively (Table I) for the temperature profiles for high latitude cold winter and summer shown in Figure 2a. The measured temperatures of 230°K within the belt 40° S to 25° N are 3°K higher than those computed (Table I) for the tropical temperature profile shown in Figure 2a. This disagreement with the computation seems to be consistent with the cases at 60° N and 60° S where the measured temperatures were 2°K too high. The reason for this consistent discrepancy could be due to a number

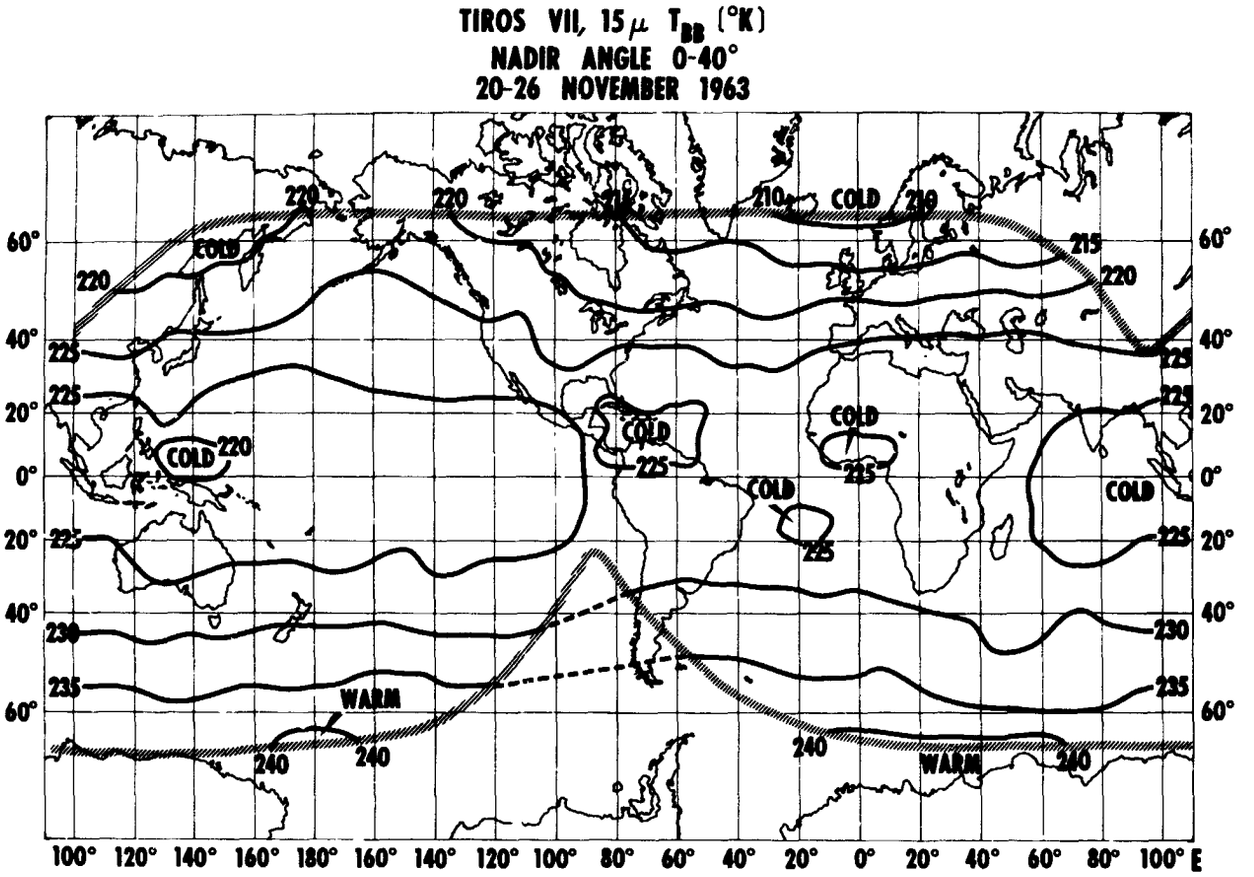

FIGURE 6.—Quasi-global map of 15μ equivalent blackbody temperatures averaged over the week 20–26 November 1963; nadir angle 0°–40°. Radiation data cannot be obtained outside the area enclosed by the dashed border.

of assumptions contained in the radiative transfer calculations which may have resulted in the computed values of T_{BB} being several degrees too low.

A coarse picture of the temperature gradient with altitude can be obtained by comparing Figures 3a and 3b. In Figure 3b, temperatures measured at nadir angles between 52 and 58 degrees were plotted. The weighting functions in Figures 2b and 2c show that all measurements shown in Figure 3b reflect temperatures at altitudes approximately 3–4 km higher than the temperatures shown in Figure 3a. Thus, by comparing Figures 3a and 3b, one may distinguish three categories in the temperature profiles:

1. Increasing temperatures with altitude between 15 and 35 km where the measured temperature differences are positive.

2. Decreasing temperatures with altitude between 15 and 35 km where the measured temperature differences are negative.

3. Isothermal regions between 15 and 35 km if the temperature differences are close to zero. It can be seen that differences of about +2°K occur in the tropics where strongly positive temperature gradients with altitude prevail. This difference agrees reasonably well with the values calculated for a tropical profile (Table 1). Over the higher northern latitudes (summer) moderately increasing temperatures with altitude and over high southern latitudes (winter) isothermal temperatures are suggested. This is in fair agreement with the calculations (Table I).

B. Seasonal Reversal, September–October 1963

As the solar illumination gradually becomes symmetrical with respect to northern and southern hemispheres during September, 1963, temperature patterns at high latitudes markedly reflect the resulting change in solar heat input. In some areas, this change takes place rapidly while other regions undergo a much slower transition. During the first two months following the

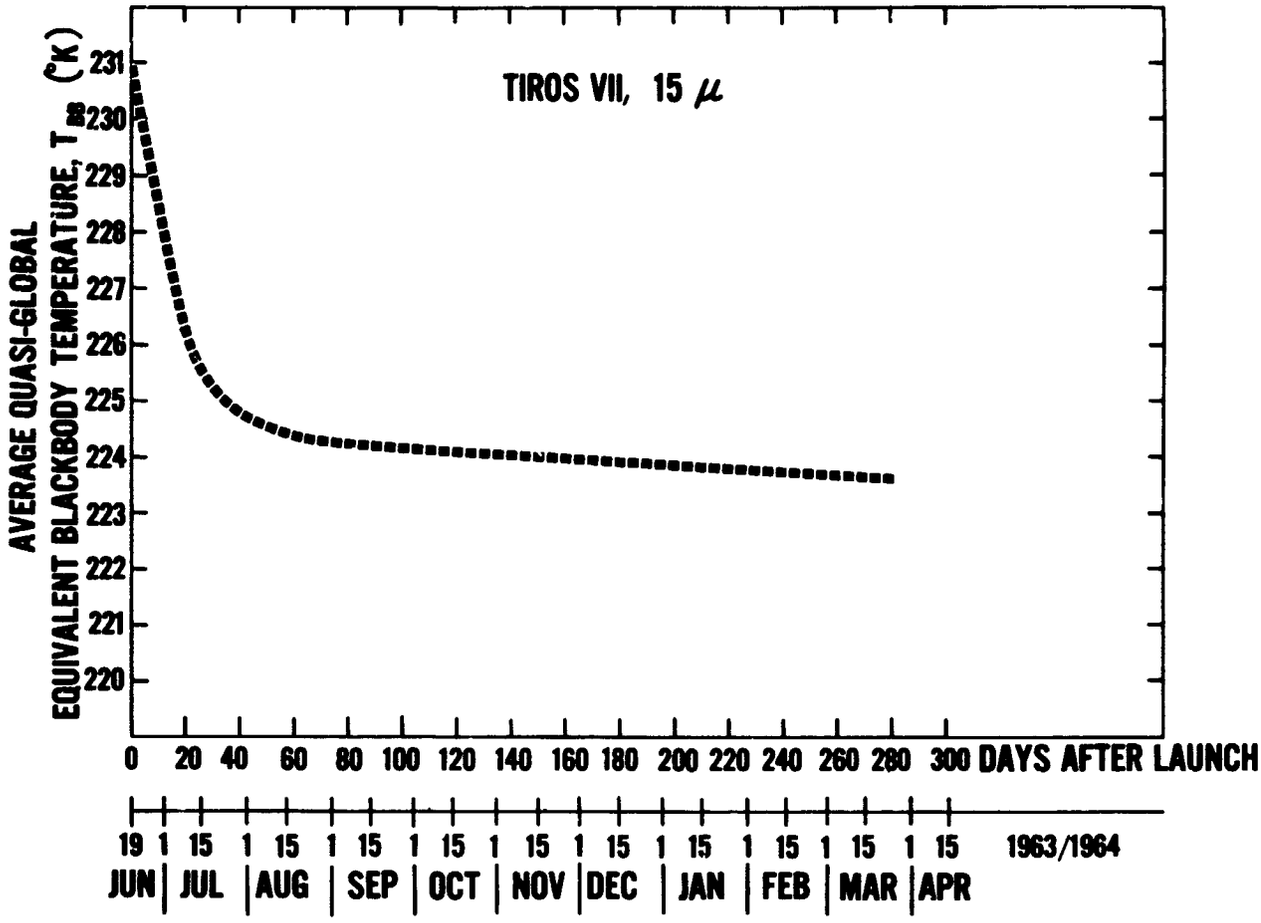

FIGURE 1(b).—Average quasi-global equivalent blackbody temperatures vs. time. The heavy dashed curve indicates the derived apparent degradation in the instrumental response.

solstice, there were practically no temperature gradients along any given latitude circle in the northern hemisphere; but strong longitudinal temperature patterns begin to develop now during the transitional season, especially after the September equinox. During July and August, the temperature patterns remain essentially the same as those during 19–25 June, shown in Figure 3a. There is one important change, however, which exhibits the same characteristics as similar changes observed on measurements in other spectral regions in previous TIROS satellites (References 7 and 8). *All* measured temperatures over the entire world seem to decline during the first three weeks of observation. It is extremely probable that a gradual degradation in the response of the radiometer is the cause for this decline. By mid-July 1963, the magnitude of this sensitivity decrease is about 7°K. After that, the degradation seems to have leveled off and continued at a much lesser rate. An approximate time history of this instrumental degradation based on the preliminary information available at this time is given in Figure 1b. A more complete version will be given in the TIROS VII Radiation Data Catalog and Users' Manual (Reference 4). An appropriate correction based on Figure 1b should, therefore, be added to all temperature measurements quoted thereafter and shown in the maps, Figure 4 to 12. Although this degradation leaves some uncertainties in the exact absolute magnitudes of the temperature measurements, it does not appreciably affect the ability to assign the appropriate temperature profile (Figure 2a) to a measurement at a given location or the implications drawn from the distribution of relative temperature patterns.

The first indication of any significant change in the post solstice temperature pattern occurs during the week 28 August to 3 September: the temperatures at high northern latitudes decrease by about 5°K to a temperature of about 228°K (+7° correction) at 60° N. At northern

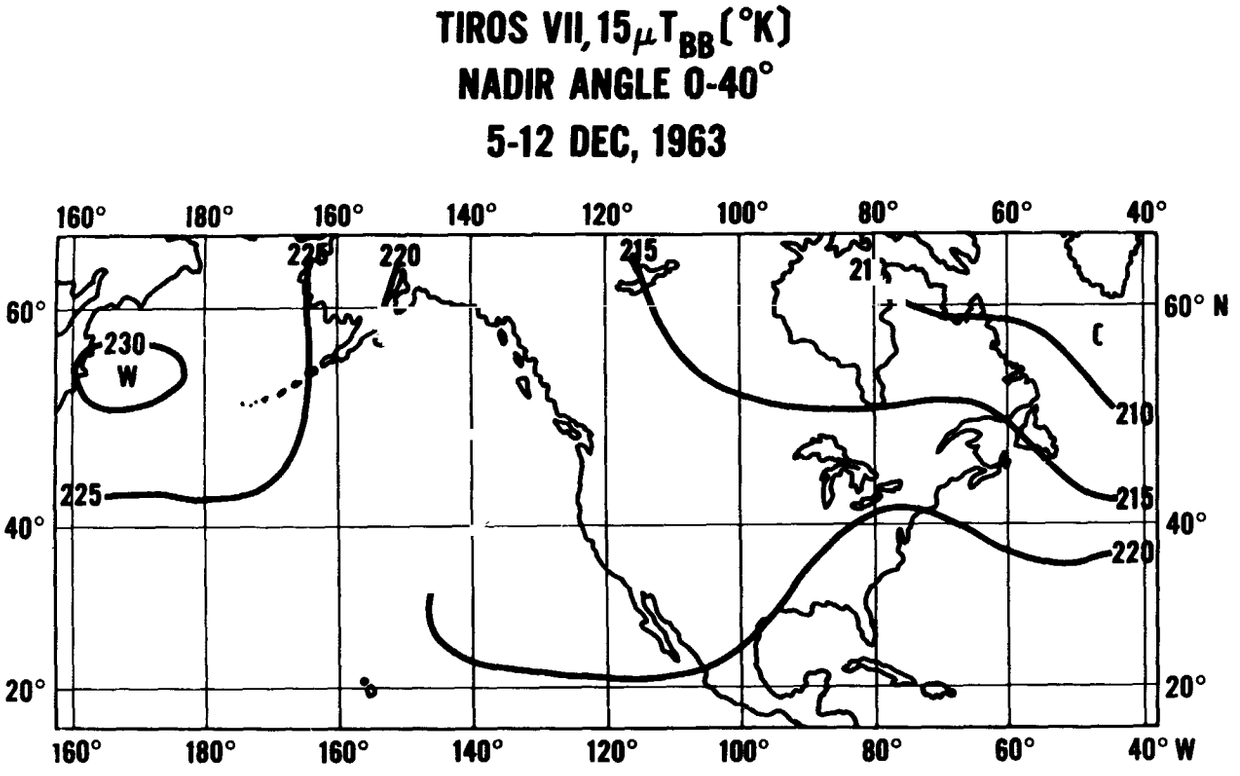

FIGURE 7(a).—Map from the North Pacific to the North Atlantic of 15μ equivalent blackbody temperatures averaged over the week 5–12 December 1963; nadir angle 0°–40°.

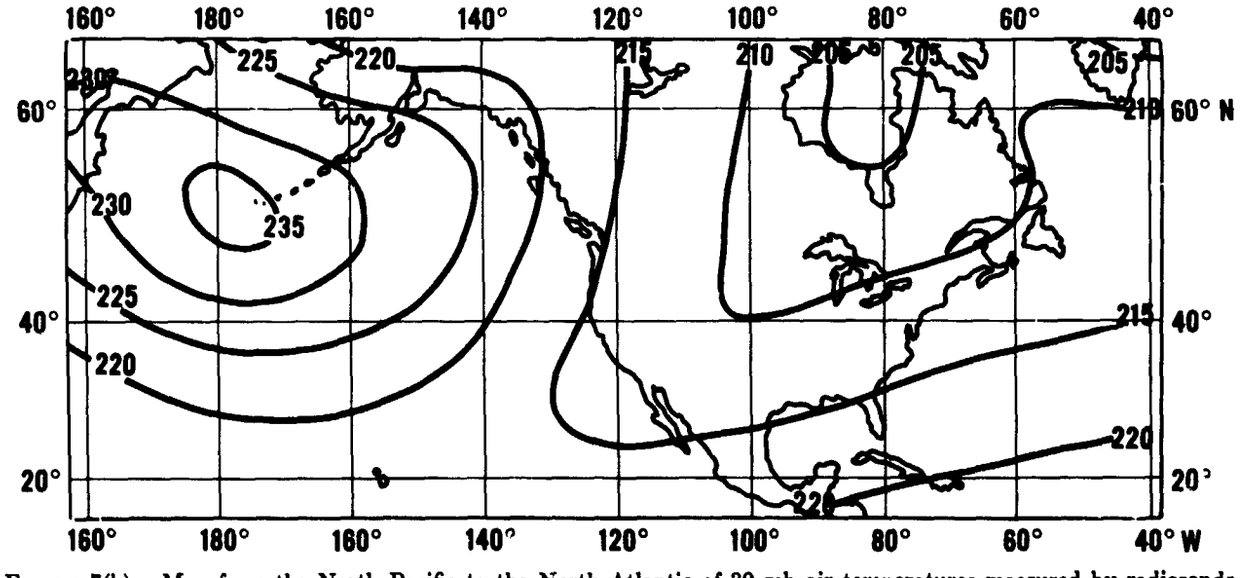

FIGURE 7(b).—Map from the North Pacific to the North Atlantic of 30 mb air temperatures measured by radiosonde balloons averaged over the week 5–12 December 1963 (Reference 16).

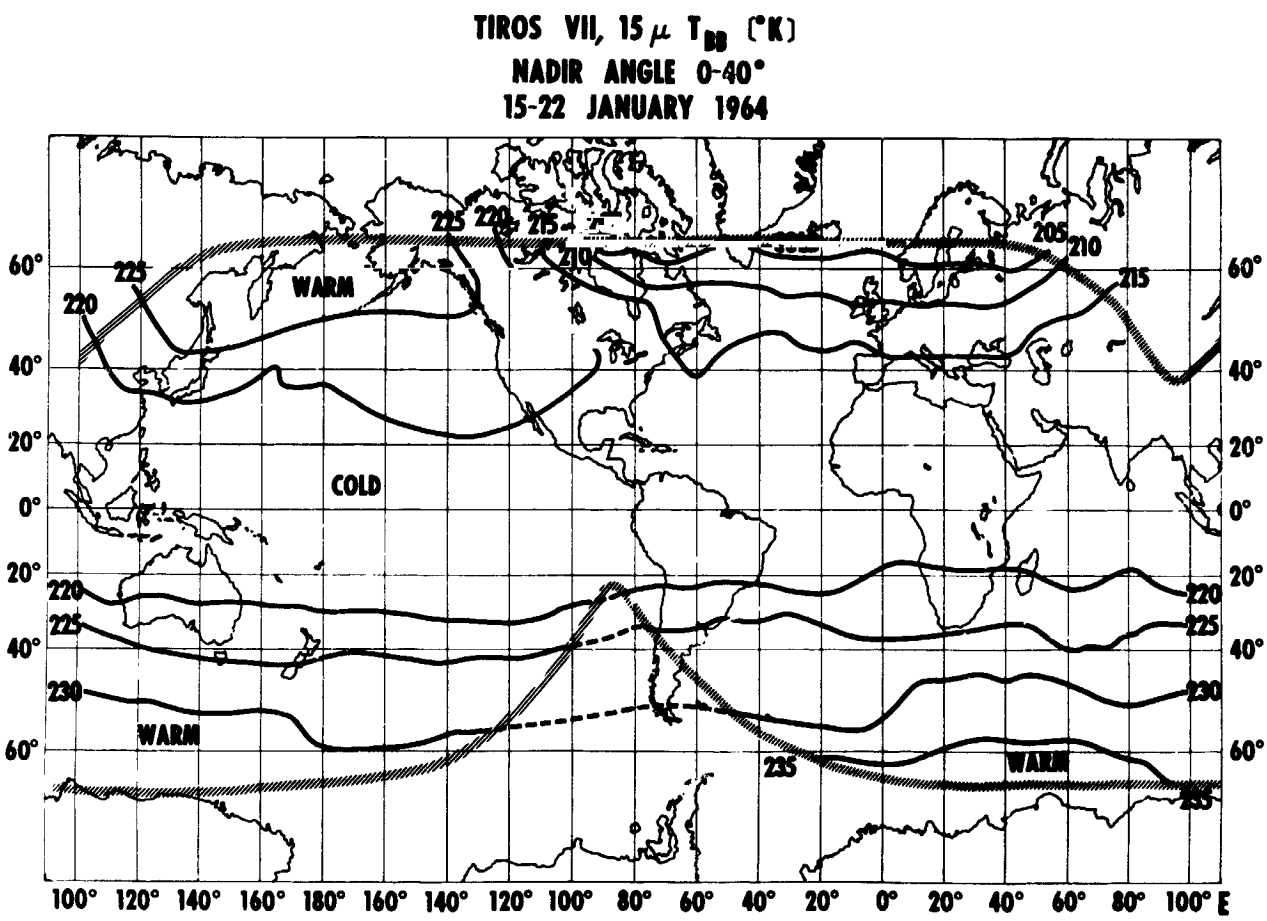

FIGURE 8(a).—Quasi-global map of 15μ equivalent blackbody temperatures averaged over the week of 15–22 January 1964; nadir angle 0°–40°. Radiation data cannot be obtained outside the area enclosed by the dashed border.

mid-latitudes (20°−50° N) there is also a slight temperature decrease from the summer (19–25 June) conditions. However, here this decrease does not take place uniformly at all longitudes. There are pocket-like regions where warmer temperatures seem to persist longer than over other regions causing some inhomogeneities in contrast to the quite uniform zonal pattern observed in June. Going southward, temperatures in general decrease very gradually from about 228+7°K at 60° N to about 223+7°K at 40° S with the latter temperatures prevailing over most of the zone from about 25° N to 40° S. From there southward temperatures decrease rapidly with latitude. Thus, the remainder of the southern hemisphere remains essentially unchanged, still reflecting typical winter conditions (205+7°K at 60° S) except for a warm region of 225+7°K, which developed during later winter over the Indian Ocean between 40° to 50° S. The disturbance noted during June at these latitudes over the western South Pacific has grown throughout July and early August, and a warm region extends now over the entire Indian Ocean showing a definite longitudinal pattern. For example, temperatures over the southern Indian Ocean at 60° S are about 216°+7°K. At the same latitude over the Atlantic and central South Pacific, temperatures are 213+7°K and 203+7°K respectively.

During September, the European and West Asian portions of the northern hemisphere and parts of North America begin to cool off rapidly. There temperatures at 60° N have cooled to about 223+7°K while over the northwest Atlantic and North Pacific somewhat warmer temperatures still prevail (228+7°K) during the week of 11–18 September (Figure 4). At the same time, the breakdown of the winter over the southern hemisphere is gaining impetus. The same, even intensified longitudinal patterns as observed in

August are apparent. Temperatures in the Indian Ocean warm area amount up to 234+7°K. This area has now spread out between the longitudes of 95° to 180° E along the 50th parallel, yet temperatures at this latitude over the South Atlantic and the eastern South Pacific still remain relatively cold (220+7°K). Temperatures at low and mid-latitudes, in general, range around 225+7°K (Figure 4).

The week following the equinox (25 September–1 October) shows that the temperature gradients between the two hemispheres (Figure 5) have reached their minimum during this transition period. With the exception of the very warm region at 50–55° S over the Indian Ocean reaching maximum temperatures of 236+7°K at 70° E temperatures over the entire quasi-globe are nearly constant at 225+7°K. It is significant to note that at most longitudes the temperature gradient along a given latitude belt can now be much greater than gradients between 60° N and 60° S: temperatures along 50° S vary from 236+7°K at 70° E to 223+7°K near 170° W, while along the 180th meridian, for instance, temperatures at 60° S are about 222+7°K, at 60° N about 228+7°K and at the equator about 223+7°K. This is a total variation of 6°K along the meridian compared to a variation of 13°K along the 50° S parallel (Figure 5). The phenomenon of very pronounced temperature differences between the Indian and Pacific Oceans at all latitudes between 40° S and 65° S persists during the entire transition period from winter to summer. The maximum temperature difference is about 15°K throughout this time, with the Indian Ocean area showing the warmest and the eastern South Pacific showing the coldest temperatures (Figure 5). This phenomenon first appears in large scale during the middle of August and lasts until about 20 October. During early and middle October, the eastern portion of the southern hemisphere (40 W to 120 E) is relatively warm (230+7°K at 60° S) with a warm center of

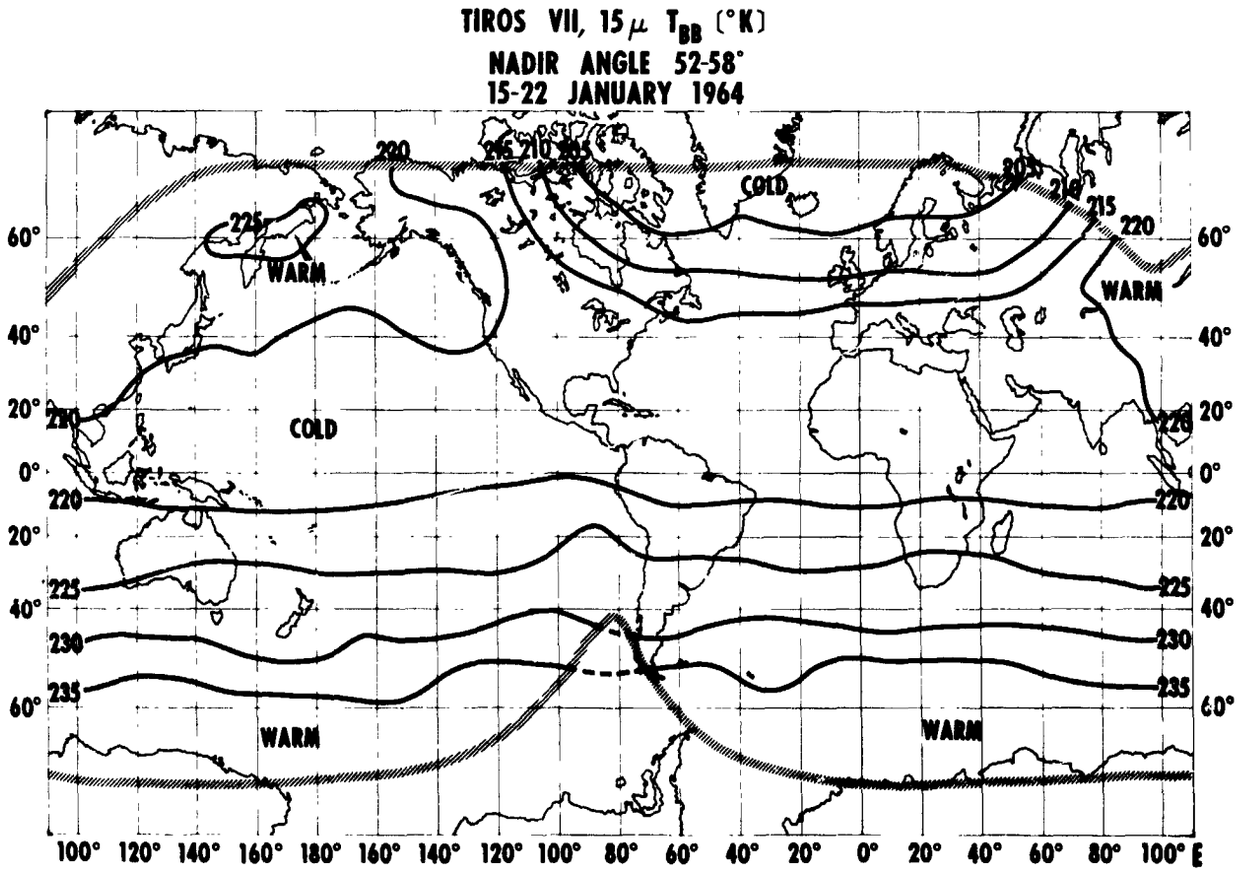

FIGURE 8(b).—Quasi-global map of 15μ equivalent blackbody temperatures averaged over the week 15–22 January, 1964; nadir angle 52°–58°. Radiation data cannot be obtained outside the area enclosed by the dashed border.

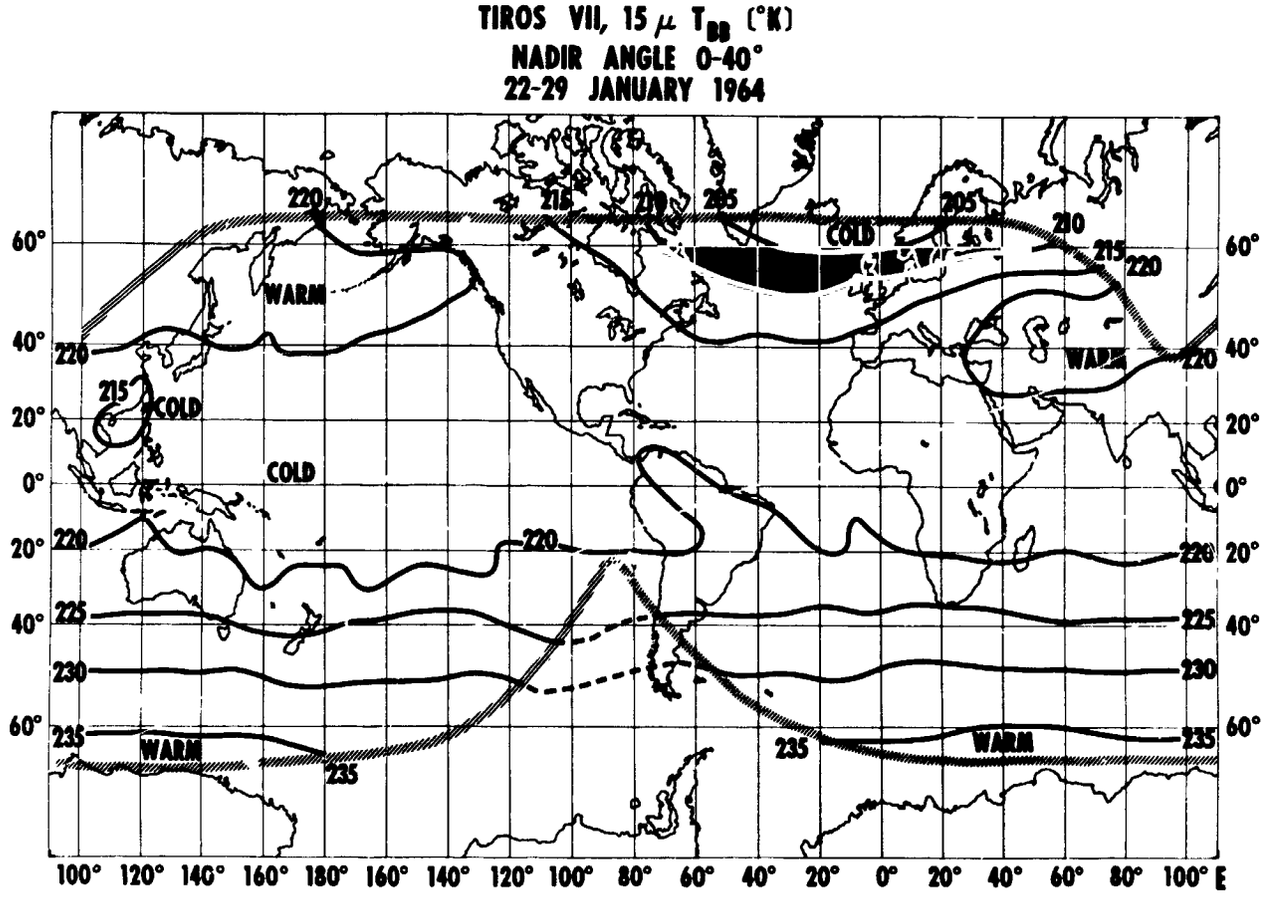

FIGURE 9(a).—Quasi global map of 15μ equivalent blackbody temperatures averaged over the week 22–29 January, 1964 nadir angle 0°–40°. Radiation data cannot be obtained outside the area enclosed by the dashed border.

234+7°K at 80° E, while the western portion remains relatively cold with the cold center at 220+7°K at 170° E. During late October, the week of 23rd to 29th, the entire southern hemisphere finally achieves a typical summer temperature pattern with wide and uniform latitudinal temperature belts ranging from about 230+7°K at 60° S to about 225+7°K at 30° S. There is a uniform belt with temperatures of almost exactly 225+7°K between 30° S and 30° N. Over the Atlantic, Europe and Western Asia, temperatures drop rapidly from 225+7°K at 30° N to 215+7°K at 60° N, while over the Pacific they remain at 225+7°K up to 60° N.

During the entire fall transition period, the north Pacific area has not cooled off as rapidly as the rest of the northern hemisphere and in general remains warmer throughout much of the winter. During the course of October, this pattern intensified whereby temperatures in all northern regions except over the north Pacific and eastern Asia continue to decline. Finally, at the end of October, as stated above, the northern hemisphere shows a typical winter pattern with the same tight gradients with latitude as observed three months previously in the southern hemisphere. At 60° N, temperatures are uniformly cold (215+7°K) over Eurasia, the North Atlantic and North America, but warm over Alaska and the Bering Sea (225+7°K). The global picture does not change appreciably between the end of October and the week 20–26 November shown in Figure 6. Although the warm area (224+7°K) over the North Pacific has somewhat diminished in size compared to the end of October, and it is now located over the Gulf of Alaska, the isotherms over the area still show a very definite departure from a zonal pattern and run northwest to southeast over North America and northeast to southwest over east Asia. While temperatures are still uniform with latitude over the Atlantic and Eurasian continent and range from 213+7°K at 60°N

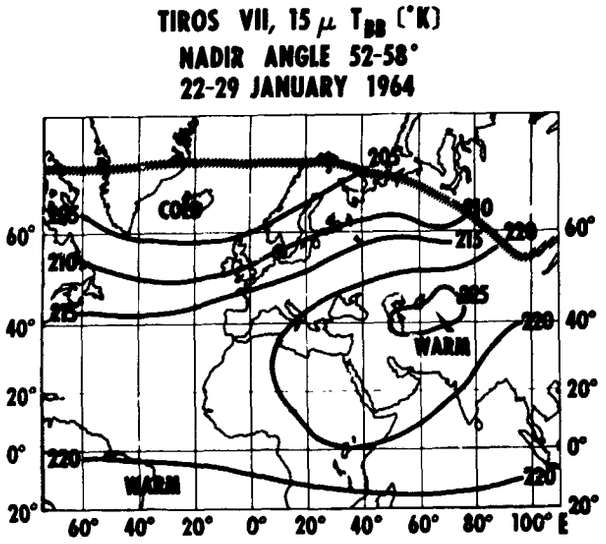

FIGURE 9(b).—Regional map of 15μ equivalent blackbody temperatures averaged over the week 22–29 January, 1964; nadir angle 52°–58°. The effects of a stratospheric warming over Eastern Europe are illustrated. No essential change in the temperatures occurred in other areas of the quasi-globe relative to Figure 8(b).

to 225+7°K at 40° N, the summer temperature pattern in the southern hemisphere is perfectly uniform with latitude and temperatures range from 235+7°K at 60° S to 225+7°K at 25° S (Figure 6). This pattern is identical to the temperature pattern during June, however, with northern and southern latitudes reversed.

C. The "Aleutian Anticyclone", December 1963

An unexpectedly warm stratosphere occurring as a regular climatological feature during winter in the general area of the Aleutian Island chain has long been recognized as the cause of a strong anticyclonic stratospheric circulation system in that area (Reference 10). Such circulation is unusual because in winter one would expect a very cold stratosphere resulting in a cyclonic circulation symmetric around the winter pole. Indeed, this cyclone exists, but in the northern hemisphere during mid-winter it is strongly disturbed and displaced by the Aleutian anticyclone. The morphology of this stratospheric warming over the North Pacific has received much attention in the past and a number of theories have been advanced attempting to explain its origin on the basis of dynamic processes (Reference 11). The satellite temperature measurements made it possible to follow the variation of mean temperatures in the lower stratosphere over this entire region throughout the winter of 1963. Figure 7a shows the temperature measured by the satellite between 40° W and 160° E and 20° N and 65° N averaged for the week from 5 to 12 December. Globally, there is practically no change from the patterns shown in Figure 6, except that the warm North Pacific region, which previously had remained at higher temperatures because it simply cooled slower than the other areas, has now actually warmed between the end of November and early December. It is centered at the end of the Aleutian Island chain and stands out clearly with temperatures of 232 +7°K. An analysis of temperatures at the 30 mb level from conventional radiosonde observations analyzed and obtained from the Freien Universität Berlin for the same area and time is shown in Figure 7b for comparison. The excellent agreement in the patterns between the two maps can serve as a measure of the validity of the satellite data. As can be seen from Figures 8, 9, 11, and 12, the Aleutian warm region is a permanent feature of the entire winter from the week of 5–12 December on. However, although temperatures within the warm center had not shown an

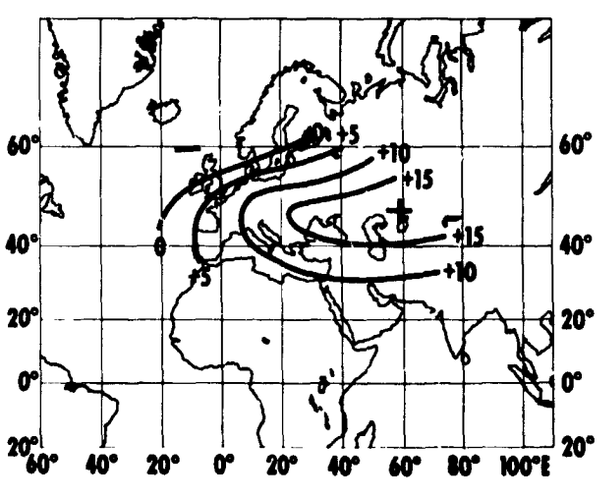

FIGURE 10.—Regional map of the differences between the 15μ equivalent blackbody temperatures measured on 27 January 1964 and those averaged over the week 9–15 January; nadir angle 0°–40°. The effects of a stratospheric warming over Eastern Europe are illustrated.

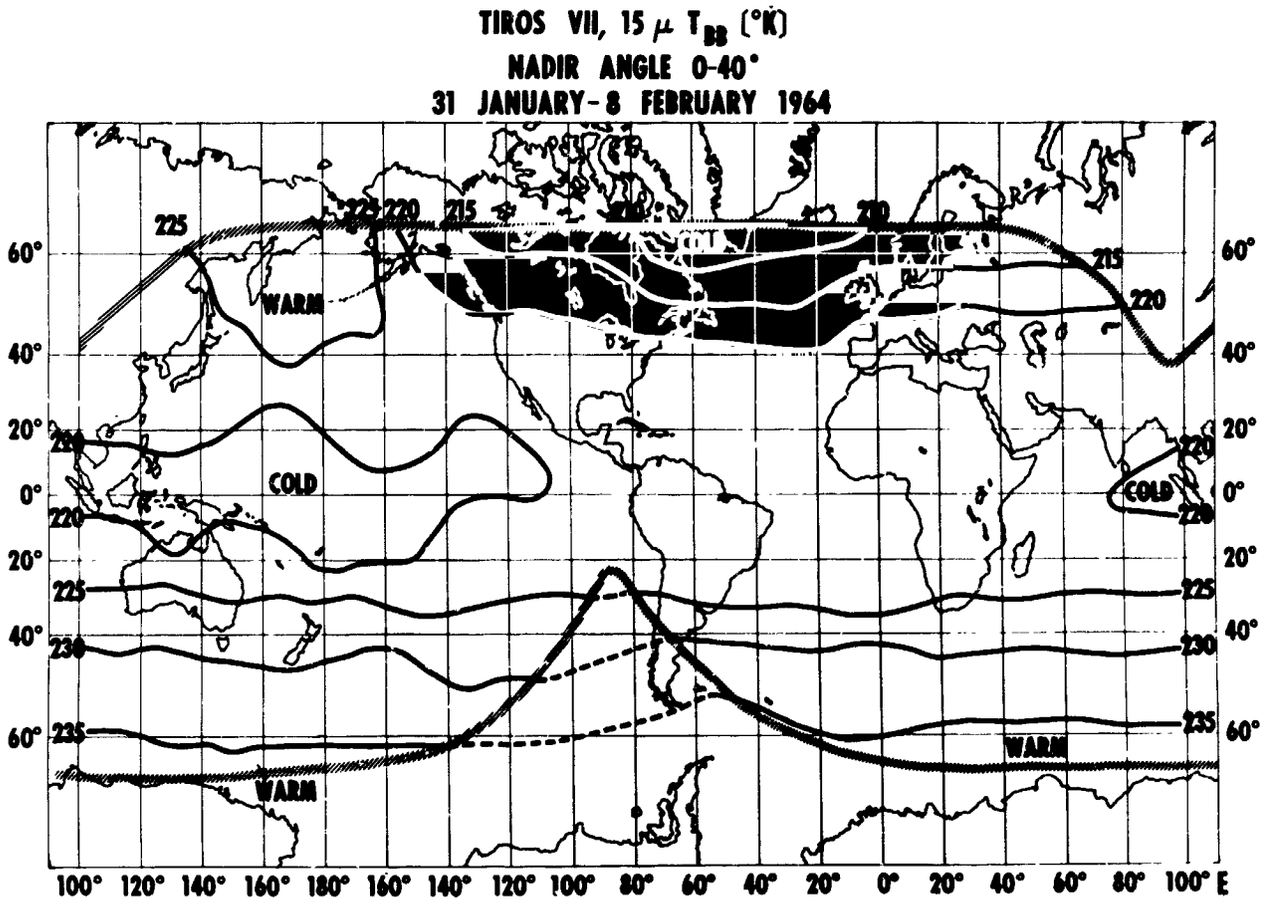

FIGURE 11(a).—Quasi-global map of 15μ equivalent blackbody temperatures averaged over the week 31 January-8 February 1964; nadir angle 0°–40°. Radiation data cannot be obtained outside the area enclosed by the dashed border.

actual increase until 5–12 December, a warm area in one form or another was present since the end of summer over the North Pacific as described above and shows in Figures 4, 5, and 6. This means that during this year the winter anomaly over the Pacific, though variable in extent during early winter, grows directly out of the summer conditions without ever reaching as low temperatures as other portions of the northern hemisphere do. Although, during early December, the system takes on a more permanent form and location and intensifies somewhat, it originated not because of a sudden heating phenomenon during winter, but simply because it refused to cool off at the end of summer. Naturally, there must be a mechanism to maintain the higher temperature during winter, while other regions at equal latitudes cool rapidly. It should be noted that those dynamic mechanisms which would have to depend on the existence of the complete winter cyclone could not explain the warm regions which already exist even before the cyclone is fully established. It might be interesting to investigate mechanisms by which the warm regions can be maintained throughout the winter by absorption of infrared radiation.

The satellite measurements show that the situation in the northern hemisphere is actually not vastly different from the southern hemisphere where a warm region over the southeastern Indian Ocean, though not quite as intense as the Aleutian one, persisted throughout the winter and then spread to make one half of the hemisphere almost 15°K warmer than the other. In the northern winter, almost a mirror image of this process occurs: the Pacific is warm and the Atlantic and Eurasia are cold, while in the south the Pacific is cold and the Atlantic and Indian Ocean areas are warm. In the north, the temperature gradients between warm and cold regions are somewhat greater (about 20°K between 180° W and 40° W at 60° N). Of course, so far satellite data exist only for the seasonal cycle 1963/64, and the ob-

servations described here must be tested by experiments in future years.

D. Solstice, December 1963

Between November 1963 and the middle of January 1964, there is very little change from the temperature patterns shown in Figure 6. As discussed above, the Aleutian warm center becomes somewhat stronger and quite stationary during early December and, in contrast, the Atlantic and Eurasian cold regimes remained unchanged with very tight latitudinal temperature gradients and isotherms aligned with latitude during the week 15–22 January 1964 (Figure 8a). It is interesting that the temperature difference of about 15°K between 60° N and the tropical belt over the eastern portion of the northern hemisphere is less than the longitudinal temperature difference between the Aleutian warm center and the North Atlantic at 60° N. A similar situation existed in the southern hemisphere at the end of winter (Figure 5); but during the solstice, the Australian warm area did not extend to such high latitudes as the Aleutian area does. As shown in Figure 8a, the mid-latitude and tropical regions have cooled considerably; and the temperature between 25° S and 40° N is now about 218+7°K, while earlier temperatures in the same zone ranged near 225+7°K. This remarkable cooling over so wide an area is particularly significant since it precedes by about one week the occurrence of a stratospheric warming over western Asia. Instrumental degradation cannot be responsible for such a temperature decrease, since Figure 12 does indicate higher temperature again in March. Also, ever since November temperatures at high southern latitudes remained unchanged. Relatively moderate and very uniform temperature zonal temperature gradients exist at all longitudes. Temperatures at 60° S are 235+7°K.

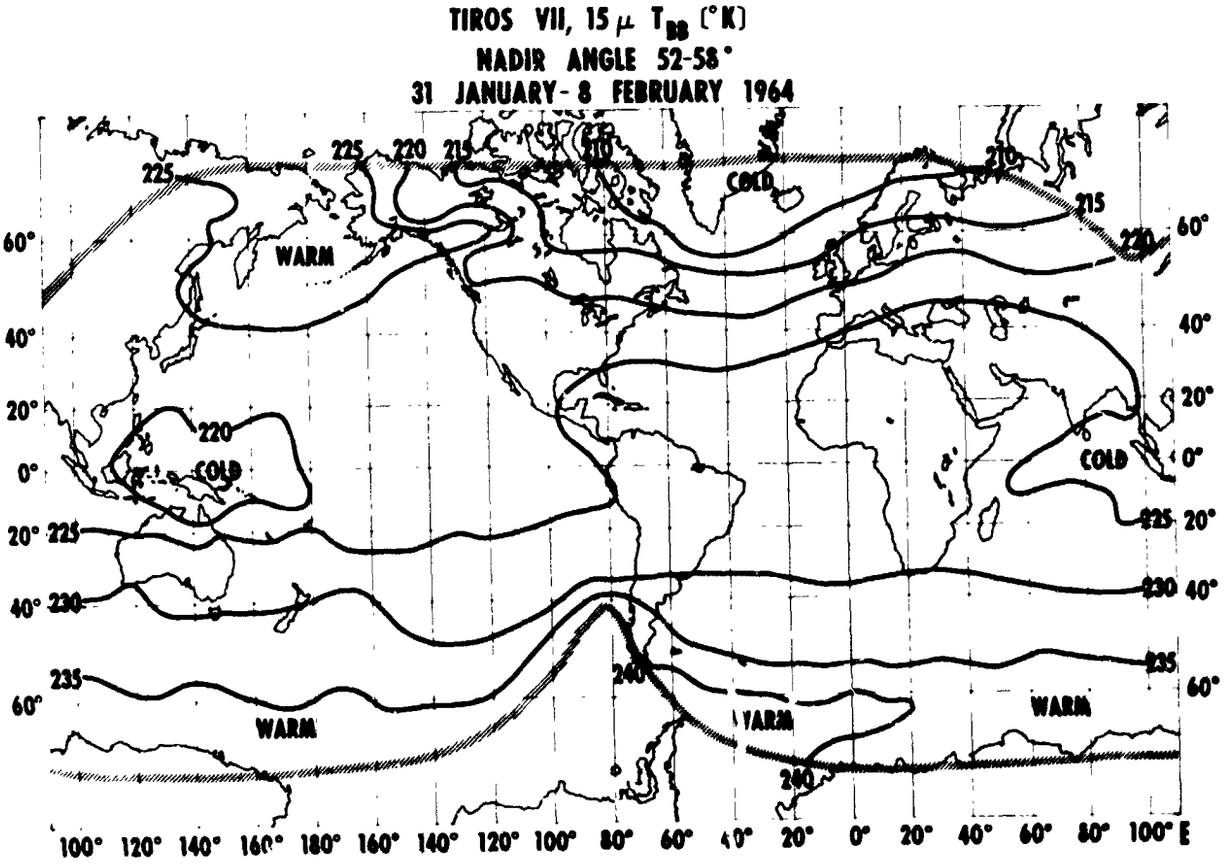

FIGURE 11(b).—Quasi-global map of 15μ equivalent blackbody temperatures averaged over the week 31 January–8 February 1964; nadir angle 52°–58°. Radiation data cannot be obtained outside the area enclosed by the dashed border.

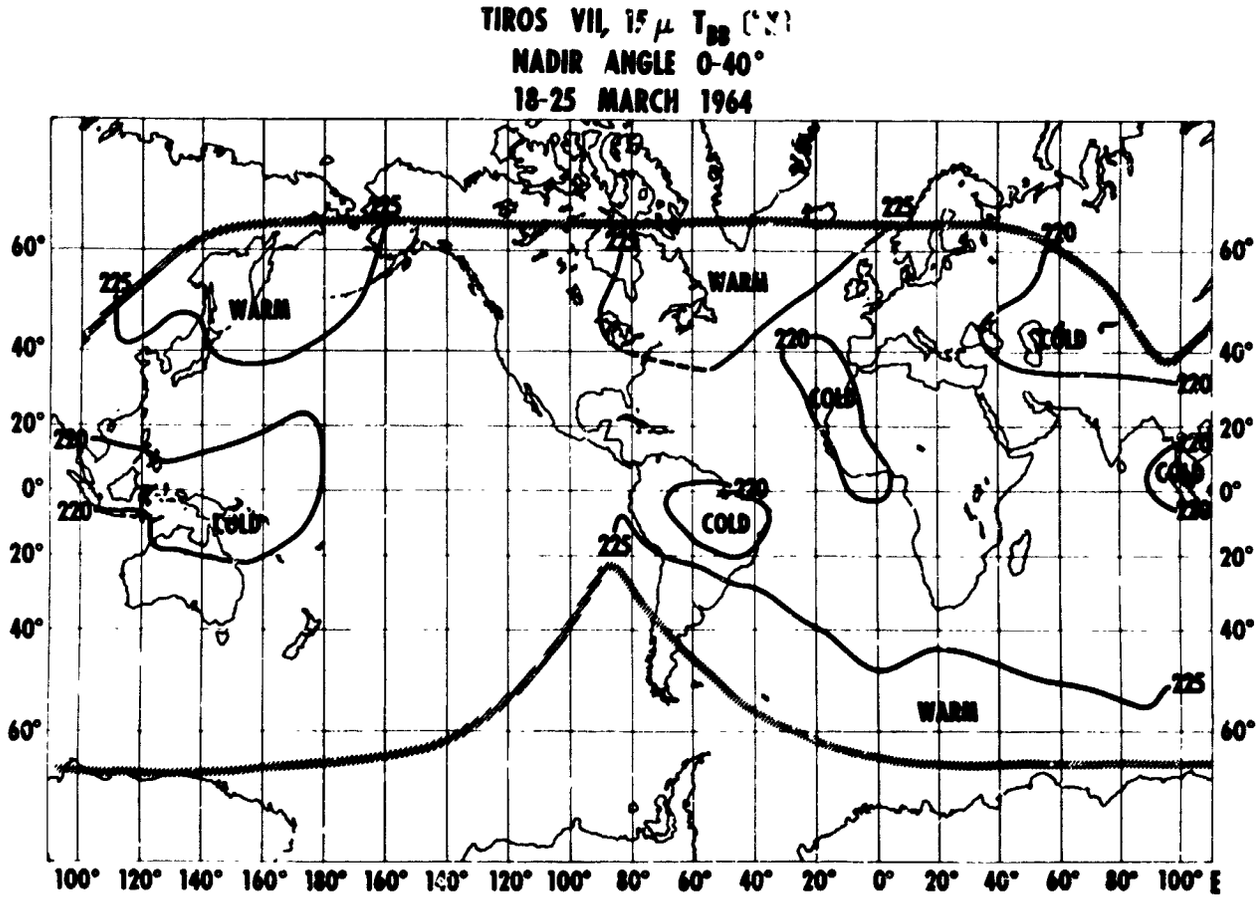

FIGURE 12.—Quasi-global map of 15μ equivalent blackbody temperatures averaged over the week 18–25 March, 1964; nadir angle 0°–40°. Radiation data cannot be obtained outside the area enclosed by the dashed border.

Temperatures of 231+7°K at 50° S and of 206+7°K at 60° N (eastern portion only) are compatible with the computed temperatures of 238 and 213°K respectively for the "summer" and "cold winter" profiles (Table I). Temperatures calculated for the "tropical" profile (227°K, Table I) are about 2°K higher than those measured in the now cold mid-latitude belt (218 +7°K). Mean temperatures of 232+7°K in the center of the Aleutian warm region measured during December suggest that the average temperature of the stratosphere in the 15 to 35 km region was about 12°K higher than that shown in the "warm winter" profile of Figure 2, which yields a mean temperature of only 229°K (Table I). Of course, such a temperature profile in this partic[illegible]ar altitude region is merely postulated since, for example, a low average stratospheric temperature of 205°K in the altitude region from 15 to 35 km, such as shown in the "cold winter" profile, Figure 2a, could be balanced by an extraordinarily high average temperature of 300°K in the region from 35 to 60 km to produce the measured radiation temperature of 239°K. But, such a temperature profile is much less probable than the one postulated. The validity of the assumption of an average stratosphere temperature increase of 12°K between 15 and 35 km is also suggested by comparing the satellite measurements at low nadir angles (0–40°, Figure 8a) to those at high nadir angles (52–58°, Figure 8b). Temperatures over the Aleutian warm area are practically the same at both nadir angle ranges indicating a nearly isothermal or at least a very slowly varying temperature gradient with altitude in the region where the weighting functions $\Psi(h)$ are at their maximum (15–35 km, Figures 2*b* and 2*c*). A temperature profile such as the one mentioned above with a mean temperature of 205°K between 15 and 35 km and 300°K between 35 and 60 km would produce a difference of 9°K between the radiation temperatures measured at 0° nadir and

at 58° nadir angle. Figures 8a and 8b, however, indicate no temperature difference at all over the Aleutian warm area. Thus, one finds that the difference in the mean temperatures between 15 to 35 km level and the 35 to 50 km level cannot be excessively large, and with that restriction, a temperature increase of 10°K for the standard "warm winter" profile from 15 to 35 km follows for the North Pacific area. Similarly, one finds that there is no temperature differences for the two nadir angles over the North Atlantic and Northern Europe (Figures 8a and 8b) which agrees well with the calculated differences of 1°K for the "cold winter" profile. The larger temperature differences over the tropics—the 220°K isotherm is about 10° further north in Figure 8b than in Figure 8a—indicate the rapid temperature increase with altitude above 15 km and agree well with the computed difference of 4°K for the "tropical" profile (Table I); while the calculated values of 238 and 240°K for "high latitude summer" (Table I) agree well with the observed temperatures (+7° correction) and temperature differences between 50 and 55° S.

This picture has changed considerably during late January (Figures 11a and 11b) where temperature differences at mid-latitudes and in the tropics over the entire eastern hemisphere are as high as or exceed the differences observed previously within the tropics. Such large differences exceeding 5°K extend particularly into North Africa, the eastern Mediterranean and the Near East (Figures 11a and 11b). This indicates that neither the "tropical" nor the "summer" temperature profiles (Figure 2a) apply in this case. In that area, temperatures at 15 km must be somewhat higher than those given by the "tropical" profile; and there must be a pronounced increase of temperature with altitude resulting in a very warm upper stratosphere, i.e. a very strong vertical temperature gradient between the lower and upper stratosphere. It is significant that this change has occurred over the area into which the sudden warming, described below, has moved in its decaying stages.

E. Sudden Warming, January 1964

The type of temperature measurement from a satellite described here was expected to be most useful for the detection of the occurrence and the observation of the behavior of stratospheric warmings. These warmings were first observed over Berlin by Scherhag (Reference 12) and have since then been the subject of intensive observation and analysis (Reference 13). The sudden warmings have now been observed almost every year during the northern hemisphere winter and, during their occurrence, the lower stratosphere over a limited area may be heated by as much as 30°K within a few days. Causes for such warmings have thus far not been explained. In contrast to the Aleutian warm center described above, the sudden warmings show no regularity in their time and location of occurrence. In order to be detectable by the TIROS radiometer, the warming must occur at altitudes between 15 and 35 km, or, if it occurs at other levels, it must be unproportionally intense. Calculations based on the "warm winter" temperature profile of Figure 2a show that a uniform temperature increase of 12°K between 15 and 35 km will increase the radiation temperature by 10°K, while a similar change of the temperature profile between 34 and 44 km will cause a rise in the radiation temperature of less than 1°K.

A number of small and weak warmings occurred over America and Europe during December 1963 and January 1964, but those did not penetrate to altitudes below 30 km (Reference 14). Therefore, they could not be detected by the satellite. During the last week of January (22–29), however, a warming of apparently moderate intensity occurred over the region of the Caspian Sea, extending between the Himalayan Mountains and the Black Sea (Figure 9a). Radiation temperatures over that area have increased by about 8°K over the previous week (Figure 8a). During that week (15–22 January), there was practically no indication of any disturbance in the perfect latitudinal temperature structure over that region, except perhaps for a very small area over Iran where a temperature increase of about 2–3 degrees could be observed; but in the high nadir angle measurements, there is an indication of increased temperatures over South Central Asia (Figure 8b) inferring that the subsequent warming might have originated in the upper stratosphere (above 30 km) in that area. Unfortunately, the warming developed in an area where no conventional meteorological data at these altitudes are

available, and the satellite observations provide the only method of analyzing the event. Furthermore, even the satellite observations are limited in coverage, since this area is located near the data gap over the central Soviet Union which exists because of the particular geometry of the data readout stations for TIROS (see above). The satellite data were, therefore, analyzed for individual days of 22, 24, 25, 26, 27, and 29 January. These daily analyses showed that the temperatures within the warm center were as high as 230+7°K on 29 January, but because they extended only over very small regions and because of the motion of the center from day to day, these high temperatures became obscured in the weekly averages (Figure 9a). The first definite indication of the warming occurs on 22 January, where a small and relatively weak warm center of 225+7°K appears over Pakistan, Afghanistan and Eastern Iran. This is already a few degrees higher than the average temperature over the same area for the preceding week of 14–22 January (Figure 8a). Two days later on 24 January, the warm region had spread out somewhat to the north, and the center had also moved in that direction but had not significantly intensified. On 25 January, temperatures of 225+7°K range over the entire middle East extending as far eastward as central China. The center is now just east of the Caspian Sea and has just barely reached a temperature of 230+7°K. On 26 January, the same situation prevails with the center becoming slightly warmer and larger. On 27 January, the center has grown considerably larger and temperatures of 230+7°K extend over an area of at least 30° longitude and 10° latitude northeast of the Caspian Sea. The 225+7°K isotherm has advanced to a latitude of 50° N, causing a tremendously tight temperature gradient over northern Europe where temperatures increase by more than 20°K from southern Norway to the Black Sea. Due to the warming, isotherms have been tilted to follow a course from southeast to northwest instead of the perfect eastwesterly direction still prevailing on 22 January. Finally, on 29 January a warm center extending over 10° great circle arc with temperatures of 230+7°K stretches from the Black Sea eastward to China. One 225° isotherm now runs east-west along the 40th parallel between 40° E and 80° E. The other runs southwest to northeast from the Black Sea to about 50° E and 55° N. The center is located near 65° E and 50° N. This situation is summarized in Figure 10 which shows that on 27 January the radiation temperatures had increased by 15°K over the averages for the week 9–15 January near the center and that the periphery of the warming extended as far west as the North Sea, and the Atlantic and as far south as North Africa and Arabia. Figure 11a shows that during the week 31 January to 8 February the warming had passed its climax. Rather homogeneous temperature patterns with latitude return over northern Europe and eastern Asia, but south of 40° N a broad warm area of about 223+7°K now covers the entire region between 40° N and 25° S latitude and 110° W and 80° E longitude (Figure 11a). This means that the mid-latitude belt which had cooled so drastically before the warming had been restored close to its normal temperature of about 223+7°K between 25° S and 40° N. Figures 8, 9, and 11 show that the Aleutian warm center had remained undisturbed during the entire period of the warming. On 30 January, the warming was detected by a radiosonde ascent over Berlin, the only one available for this analysis (Reference 15). This radiosonde temperature profile, when compared to a prewarming profile shows that the warming over Berlin occurred primarily above 30 km. For the week of 22–29 January, temperatures at high nadir angles are about 5°K higher than at low nadir angles not only over the warm center, but also extending far beyond the center, particularly along the southern and western periphery of the warming (Figures 9a and 9b). This means that over the center temperatures have increased not only in the lower stratosphere but more so in the upper stratosphere. The much greater extent of the warming in the high nadir angle temperature patterns compared to the low nadir angle patterns suggested that along the western and southern periphery the warming occurred only in the upper stratosphere. This confirms the above mentioned radiosonde observation over Berlin. Since the much larger warming (13°K) in the center would require an unreasonably large temperature if the warming were confined to altitudes above 30 km, and since such a strong vertical temperature gradient would be clearly noticeable as a much

greater temperature increase at the larger nadir angles, it must be concluded that the warming near the center penetrated to much lower altitudes where the Ψ functions are at maximum. If the warming occurred uniformly at altitudes from 15 to 35 km, a temperature increase of about 15°K would satisfy the radiation measurements. Such an increase is quite commensurate with a moderate stratospheric warming.

F. Equinox, March 1964

The global temperature structure undergoes a major change during the period from early February (Figure 11a) to the week of 18–25 March shown in Figure 12. The steep zonal winter time temperature gradients at high northern latitudes, particularly over the eastern hemisphere as well as the zonal summer pattern in the southern hemisphere have disappeared. The southern hemisphere has cooled considerably, and parts of the northern hemisphere have warmed. This results again, as during the September equinox, in an almost constant temperature over the entire quasi-globe. In fact, temperature gradients, longitudinally or latitudinally are even shallower than during September. Over the eastern Pacific, there is no temperature gradient at all between 60° S and 60° N, with temperatures of about 223+70°K prevailing at all latitudes. As the southern hemisphere cools, a temperature gradient along 60° S seems to develop similarly as during the previous winter. The South Indian and Atlantic Oceans are now about 5°K warmer than the South Pacific.

In the northern hemisphere near 60° the North Atlantic and northeast North America have warmed rapidly by about 20°K since February, while the region east of the Black Sea, where the sudden warming occurred in January, has returned to its pre-warming winter temperatures of 217+7°K. Temperatures in the Aleutian region have remained practically constant throughout the winter and are still at about 228+7°K. This produces temperature differences of about 10°K between the Atlantic and Pacific warm regions and central Asia at 50° N. That is the largest temperature difference found during this equinox (Figure 12). Since these data have been reduced only very recently, there has not yet been an adequate opportunity to analyze the January to March transition as thoroughly as the June to October period. Such an analysis will be made in the future.

IV. CONCLUSIONS AND SUMMARY

Satellite measurements of emitted radiation in the 15 micron carbon dioxide band have demonstrated that mean temperatures in the lower stratosphere can be mapped on a global scale. By comparing measurements at high and low nadir angles, a qualitative inference can be made about the vertical temperature gradient between the lower and upper stratosphere. Analysis of global temperature patterns from June 1963 to March 1964 revealed that temperature patterns in both hemispheres remain relatively undisturbed during summer. These patterns are oriented very precisely along latitude circles with the temperature maximum occurring at the summer pole. Near maximum temperatures are reached in the southern summer about one month after the equinox. After that, temperatures increase only slightly through the solstice and remain high until the next equinox. The northern summer could only be analyzed through its peak and declining phases, June to September 1963. Temperatures decline very slowly during the first two months following the solstice. Then, a rapid decline occurs just before the equinox. During both equinoxes, temperatures were relatively uniform and differences of about 10–15°K may exist both with latitude and longitude. Winter temperature patterns in both hemispheres exhibit strong temperature gradients between the pole and 40°, but a completely uniform pattern never exists in either winter hemisphere. A fairly uniform region with temperatures generally around 230°K extends between 25° latitude of the summer hemisphere and 40° latitude of the winter hemisphere during solstice. The satellite measurements not only permitted for the first time a continuous analysis of the southern hemisphere from June 1963 to March 1964 up to a latitude of 65° S, but also demonstrated the usefulness of uniform and continuous data coverage over the entire quasi-globe. A warm area over the Indian Ocean, though initially small, seems to play a similar role in the southern winter as the Aleutian warm center during the northern winter. During winter 1963, this warm region grew out of a disturbance in the isotherms

during June and finally divided the entire stratosphere of the winter hemisphere into a "warm" and "cold" portion with the warm portion located between Africa and Australia. Temperature differences between these warm and cold areas amounted to about 15°K and disappear with the warming of the South Pacific area during late October, giving way to the homogeneous summer pattern. Similarly, there is no homogeneous winter pattern in the northern hemisphere. A large region over the North Pacific does not cool off as rapidly after the equinox as the rest of the stratosphere. Just before the solstice, this region becomes well established and intensifies in the area where the Aleutian anticyclone is usually found.

The morphology of a stratospheric warming over southwestern Asia and its penetration to Europe was observed by the satellite indicating that heating of possibly 20°K penetrated down to at least 20 km over the center of the warming, but at the periphery warming of perhaps somewhat greater magnitude remained at altitudes above 30 km. The persistent climatological inhomogeneities of warm cells over both winter hemispheres lead to the speculation that during winter the stratospheric temperatures may be influenced by radiation from underlying surfaces, while during summer solar heating is dominant.

A study was also made of the effect of how high altitude clouds on the measured temperatures, since the weighting functions (Figure 2b) are not negligible at 10 km. The result indicated that very large and high cloud systems such as hurricanes do decrease the measured temperatures by as much as 10°K if the clouds reach above 10 km and by less than 4°K if the clouds, filling the field of view are at 6 km; but it was shown that such effects are only isolated and are averaged out by the weekly analyses which formed the basis for this investigation.

ACKNOWLEDGMENTS

Experiments resulting in findings such as the ones presented here always require the efforts of many hundreds of dedicated individuals. We gratefully acknowledge the contributions of those who have contributed to the success of the TIROS VII experiments. We are particularly indebted to Mr. Robert Hite and his team for the computational efforts in reducing the vast amount of radiation measurements to the maps presented here.

BIBLIOGRAPHY

1. Bandeen, W. R., Hanel, R. A., Licht, J., Stampfl, R. A. and Stroud, W. G.: "Infrared and Reflected Solar Radiation Measurements from the TIROS II Meteorological Satellite," *J. of Geophys. Res., 66*, 3169–3185, October 1961.
2. Hanel, R. A., Bandeen, W. R., and Conrath, B. J.: "The Infrared Horizon of the Planet Earth," *J. of Atmos. Sciences, 20*, 73–86, March 1963.
3. Bandeen, W. R., Conrath, B. J., and Hanel, R. A.: "Experimental Confirmation from the TIROS VII Meteorological Satellite of the Theoretically Calculated Radiance of the Earth within the 15 Micron Band of Carbon Dioxide," *J. of Atmos. Sciences, 20*, 609–614, November 1963.
4. "TIROS VII Radiation Data Catalog and Users' Manual," NASA/Goddard Space Flight Center, Greenbelt, Maryland (to be published).
5. Elsasser, W. M., with Margaret F. Culbertson: "Atmospheric Radiation Tables," *Meteorological Monographs*, 4, 23, 43 pp., August 1960, American Meteorological Society.
6. "TIROS II Radiation Data Users' Manual" NASA/Goddard Space Flight Center, Greenbelt, Maryland, 15 August 1961.
7. "TIROS III Radiation Data Users' Manual Supplement," NASA/Goddard Space Flight Center, Greenbelt, Maryland, 1 December 1963.
8. "TIROS IV Radiation Data Catalog and Users' Manual," NASA/Goddard Space Flight Center, Greenbelt, Maryland, 15 December 1963.
9. Bandeen, W. R., Conrath, B. J., Nordberg, W. and Thompson, H. P.: "A Radiation View of Hurricane Anna from the TIROS III Meteorological Satellite," NASA/Goddard Space Flight Center, Greenbelt, Maryland (to be published in Tellus, 1964).
10. Wege, K.: Druck-, Temperatur- und Strömungsverhältnisse in der Stratosphäre über der Nordhalbkugel, Meteorol. Abhandl. d. Freien Universität Berlin, Bd. V—, Heft 4 (1957).
11. Boville, B. W.: "What are the Causes of the Aleutian Anti-cyclone?" *Proceedings of the International Symposium on Stratospheric and Mesospheric Circulation 20 to 31 August, 1962, Berlin, Germany, Meteorologische Abhandlungen*, Institut für Meteorologie und Geophysik der Freien Universität Berlin.
12. Scherhag, R. A.: "Die Explosionsartigen Stratosphärenerwärmungen des Spätwinters 1951/52." *Berichte des Deutschen Wetterdienst in der U.S. Zone, 38*, 51–63, 1952.
13. Reed, R. J.: "On the Cause of the Stratospheric Sudden Warming Phenomenon." *Proceedings of*

the International Symposium on Stratospheric and Mesospheric Circulation 20 to 31 August, 1962, Berlin, Germany, Meteorologische Abhandlungen, Institut für Meteorologie und Geophysik der Freien Universität Berlin.

14. Teweles, S.: "Stratowarm Alerts 1964" dissemination by *IQSY* Stratwarm Agency, Stratosphere Analysis Project, U.S. Weather Bureau, Washington 25, D.C.
15. Stratospheric Analysis Chart for 1963–1964, *Meteorologische Abhandlungen*, Institut fur Meteorologie und Geophysik der Freien Universitat Berlin.
16. Cole, Allen E., Kantor, A. J., and Court, A.: "Supplemental Atmospheres," *Interim Notes on Atmospheric Properties—32* (*Rev.*), 6 June 1963, Air Force Cambridge Research Laboratories, Office of Aerospace Research, U.S. Air Force, Bedford, Mass.

N64-31317

CLOUD HEIGHTS AND NIGHTTIME CLOUD COVER FROM TIROS RADIATION DATA*

S. I. RASOOL†

Radiation data obtained from TIROS III have been analyzed, separately for day and for night, for the period July through September 1961. The global distribution of the average effective temperatures measured by the 8–12μ channel of the satellite radiometer shows a close correlation with the cloud cover data.

An estimate of the latitudinal distribution of cloud heights has been obtained using the TIROS radiation data for daytime and the distribution of cloud cover recently obtained from the TIROS photographs. Combining these values of the cloud heights with the nighttime radiation data determines the latitudinal distribution of nighttime cloud cover.

The results indicate that in the Southern Hemisphere the percentage cloudiness at night is considerably higher than in the day, while in the case of the Northern Hemisphere the cloudiness appears to decrease at night.

1. INTRODUCTION

In a recent paper, Arking (1964) has derived the global distribution of cloud cover by the analysis of TIROS III video pictures. In Fig. 7 (Curve 1) is plotted the latitudinal distribution of average *daytime* percentage cloud cover as obtained by Arking for the period of 12 July through 10 September 1961.

In the present study we attempt, using these data and the simultaneous radiation measurements by TIROS III, to derive the average latitudinal distribution of *cloud top heights* and thence the *nighttime* cloud cover. Curve 2 in Fig. 7 shows the resulting percentage cloud cover during the night as a function of latitude.

2. TIROS INFRARED DATA

The radiation instrumentation in TIROS and the physical significance of this experiment have already been described by several authors (Bandeen *et al.*, 1961; Nordberg *et al.*, 1962). Three of the five channels of the TIROS radiometer measure terrestrial radiation in the far infrared corresponding to wavelength intervals of 5.8–6.5 μ, 8–12 μ, and 7–30 μ. The other two channels record the solar radiation in the visible, as reflected by the earth, to obtain an estimate of the albedo of any region. The wavelengths of the infrared channels have been chosen so as to provide information on the temperature at different levels of the atmosphere and to give an estimate of the total outgoing radiation in the infrared. In this discussion we shall only be concerned with Channel 2, sensitive in the 8–12 μ region of the infrared.

The main absorber of infrared radiation in the earth's atmosphere is water vapor. The absorption coefficient, however, varies considerably with wavelength between 4 and 50 μ, where almost all the energy of the terrestrial radiation is confined. In the 8–12 μ spectral interval the absorption by water vapor and also by CO_2, the other important absorber of the infrared radiation, is at its minimum. Consequently, *in the absence of clouds*, Channel 2 of the satellite radiometer, measuring in this atmospheric "window," records energy originating from very near the ground corresponding to an effective temperature only ~5–10 deg K less than the ground temperature (Wark, Yamamoto and Lienesch, 1962; Prabhakara and Rasool, 1963).

Reasonably thick clouds, however, are practically opaque to infrared radiation of wavelengths >4 μ (Shiffrin, 1961). As there is very little water vapor above the clouds, and if we may assume that the albedo of the clouds in the far

*Published in *Journal of the Atmospheric Sciences*, 21(2):152–156, March 1964.

†Goddard Space Flight Center and New York University, New York.

infrared is negligible, the radiometer *in the presence of thick clouds* will record energy corresponding to the cloud top temperature. This may be as much as 40–50 deg K lower than the surface temperature.

If, therefore, for any given instant, both the TIROS measured temperatures in this "window" channel and the actual surface temperatures are available, a knowledge of the temperature lapse rate in the atmosphere will enable one to obtain a quick estimate of cloud top height. On the other hand, on a climatological basis, if the satellite-measured temperatures for a given region are averaged over a season, then the departure of this temperature from the mean ground temperature will be mainly dependent on three variables—cloud amount, cloud height, and water vapor distribution in the atmosphere. As mentioned earlier, the effect of water vapor is comparatively small, and from our knowledge of climatological distribution of the water vapor over the globe, its effect on the temperatures measured by the satellite can be accounted for.

The strong effect of clouds on the TIROS III measured temperatures in the "window" channel is demonstrated by Fig. 1. In this figure are plotted the regional and temporal averages of the temperatures measured by Channel 2 of TIROS III during daytime (0600–1800 hours Local Time) for the period of July 12 through 10 September 1961. Measurements for the polar regions are not available because the inclination of the orbit was only about 48°. The surface of the earth between 50N and 50S has been divided into a 10 deg latitude by 10 deg longitude grid, and all measurements taken by the satellite in each grid at nadir angle <25 deg, between local time 0600 and 1800, have been averaged for this period.

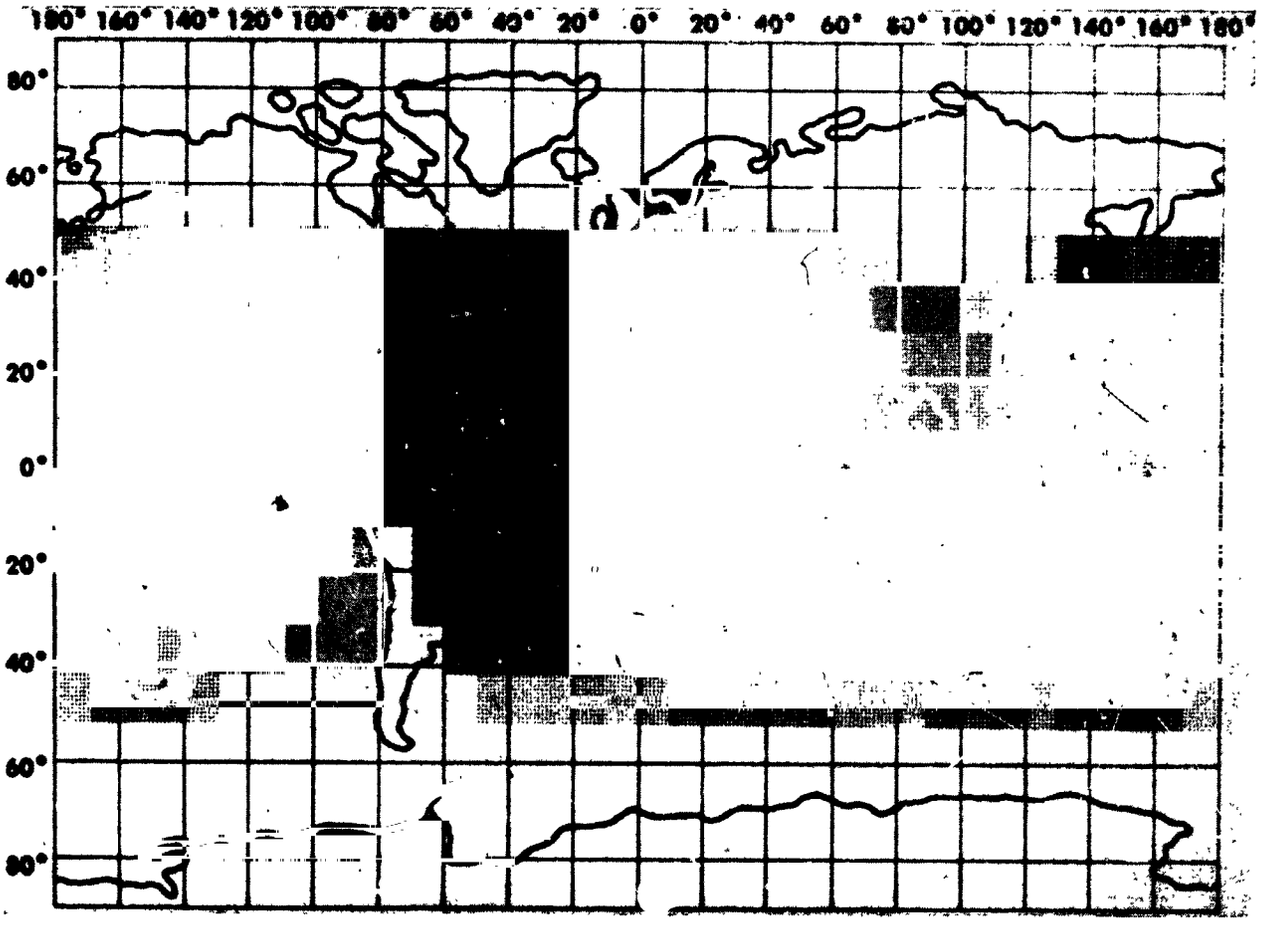

FIGURE 1.—Global distribution of average temperatures measured by Tiros radiometer channel 2 for the period 12 July through 10 September 1961. Darkest shade, $T > 295$K, lightest, $T < 255$K.

In most cases there are more than 500 observation points per grid. The observations were corrected for the instrumental degradation (Bandeen, private communication).

The very dark shades correspond to high radiation intensities with effective temperatures ranging above 290K. The lightest shades correspond to temperatures of the order of 240K. The two triangular areas, which are diagonally opposite and comprise a part of South America and Southern Siberia, have been left blank because of the unavailability of the telemetry from the TIROS for these regions.

Several interesting features are revealed by examining this figure. 1) The relatively cold temperature belt near the equator corresponds to the high cloudiness usually observed in the equatorial region. 2) The subtropical belt in each of the hemispheres show relatively higher temperatures and, therefore. probably fewer clouds than in the equatorial regions. 3) Extremely low temperatures measured over East Pakistan and India imply a heavy cloud cover over these regions which is, in all probability, the monsoon activity of this season. An almost quasipermanent cloud cover over central Africa is also indicated from this diagram.

These conclusions are supported by comparing Fig. 1 with Fig. 2 in which is plotted the global distribution of cloud cover, also in a 10×10 degree grid, taken from the climatological estimates of Haurwitz and Austin (1944). In Fig. 2, the darkest shades correspond to 20 percent cloudiness, and the lightest to 70 per cent cloudiness. The agreement in the main features of the two figures is striking, except that the TIROS III measured extremely high temperatures over the South Pacific, indicating a relatively clear area which is not noticeable in Fig. 2, undoubtedly due to lack of observational data in this region.

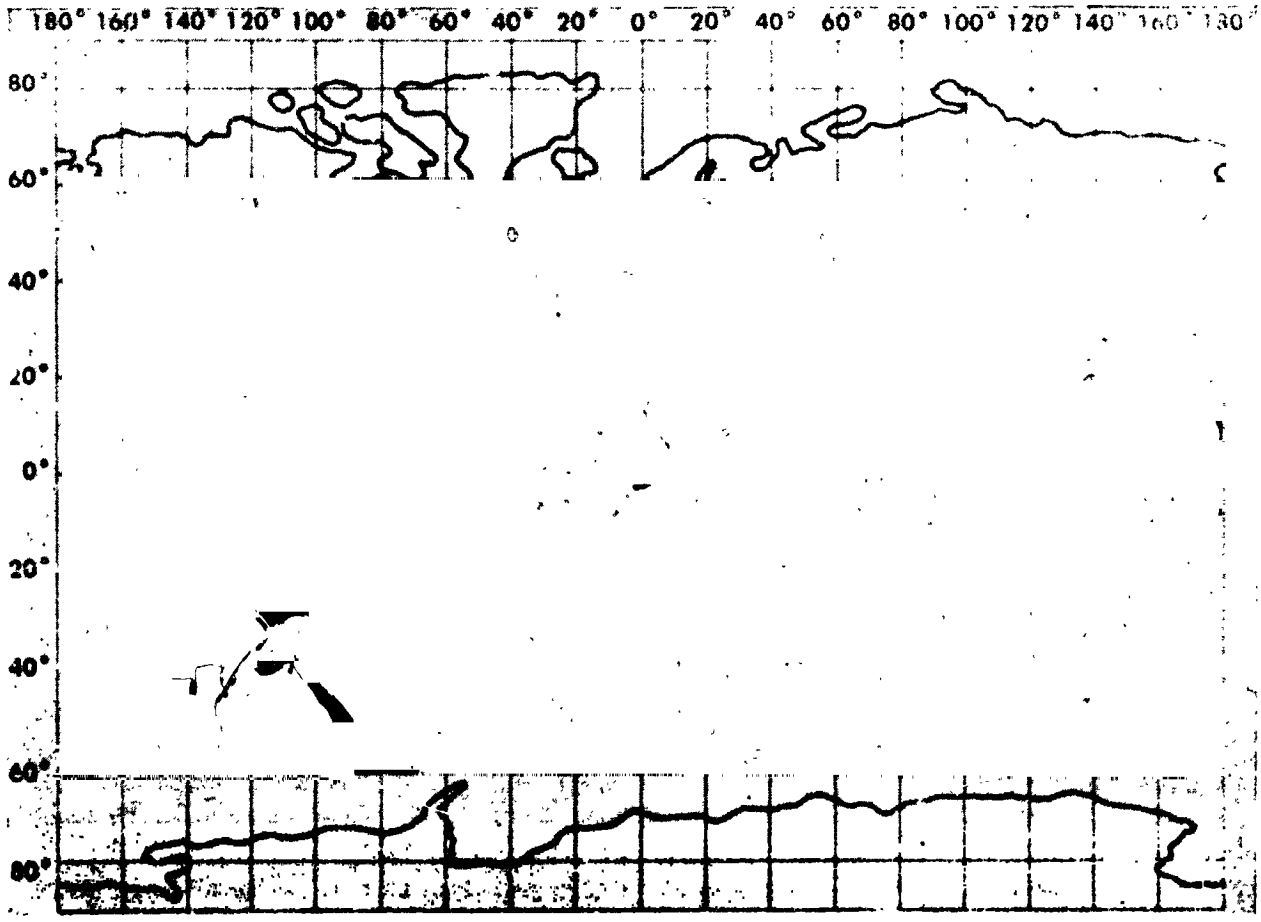

FIGURE 2.—Global distribution of average cloud cover for July (after Haurwitz and Austin, 1944). Darkest shade—cloud cover <20 percent, lightest shade—cloud cover >70 percent.

3. DEDUCTION OF CLOUD HEIGHTS AND CLOUD COVER

Although it is interesting to note the resemblance between Figs. 1 and 2, the actual derivation of cloud amounts from the TIROS radiation data is fairly involved. As mentioned earlier, several factors, viz., cloud amount, cloud height, surface temperature, vertical distribution of water vapor and of temperature, influence the 'effective' temperatures measured by the satellite. By the method described below we have, however, attempted to separate the effect of these parameters in order to obtain a reasonable estimate of cloud height from TIROS radiation data.

Using the climatological estimates of the global distribution of surface temperature (Haurwitz and Austin, 1944), the latitudinal variations in the vertical distribution of temperature (Davis, 1962, London, 1957), the total amounts of water vapor and ozone and their vertical distributions, we have constructed ten different model atmospheres which correspond to the ten latitudinal belts between 50N and 50S for the months of July and August.

The radiation flux in the 8–12 μ region, which would be emitted from such atmospheres, was then calculated following a method described in an earlier paper (Prabhakara and Rasool, 1963). The flux values thus calculated give the equivalent black body temperatures TIROS will observe above these atmospheres *if the atmosphere were completely cloudless.* Similar calculations were then repeated assuming the presence of thick clouds at various altitudes and of varying proportions. It is assumed that the clouds are completely opaque to the far infrared and the radiation is emitted only from the top of the clouds.

In Figs. 3 and 4 the results obtained for two such model atmospheres are shown. The family of five curves shows the difference (ΔT) between the surface temperature and the effective black body temperature observed by the satellite in the presence of different amounts of clouds located at altitudes of 2, 3, 4, 5, or 6 km. The intersection point of these curves with the ordinate in Fig. 3 is at 11.5 deg. This indicates that in a hot and humid atmosphere, even in complete absence of clouds, the satellite would observe an effective temperature about 12 deg lower than the surface

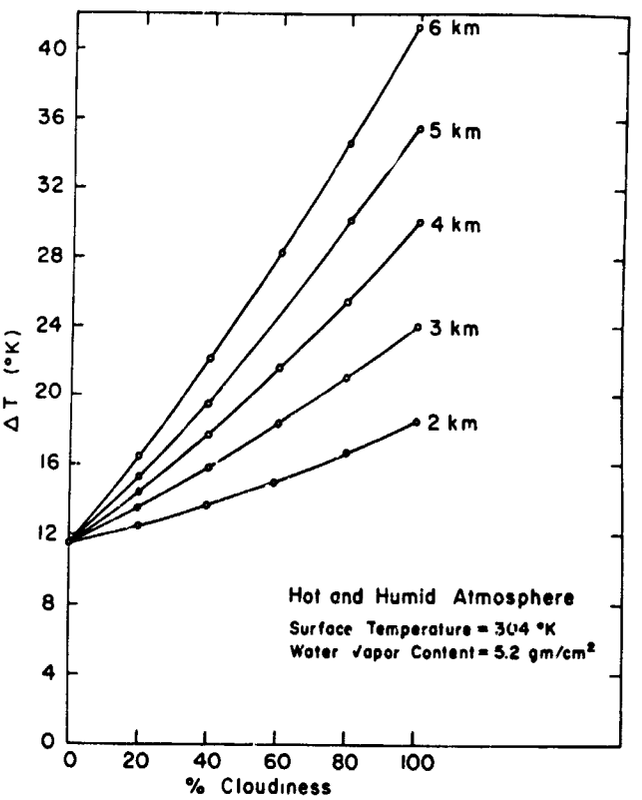

FIGURE 3.—ΔT as a function of percentage cloud cover with cloud tops at various altitudes. ΔT is the difference between the average surface temperature and the equivalent blackbody temperature measured by the Tiros III, channel 2. A case of hot and humid atmosphere.

temperature. In Fig. 4 is shown another extreme case, this time of a dry and cold atmosphere where the ΔT, in the absence of clouds, is only 3.5 deg.

If, therefore, for any given region, one has an estimate of surface temperature, of the amount of water vapor in the atmosphere and of the percentage cloud cover, then with such a family of curves, combined with the TIROS radiation data of the "window" channel, one can derive an approximate value for the effective height of the cloud tops.

In order to determine the latitudinal distribution of the effective cloud heights for the months of July and August 1961, we calculate the following parameters for each 10-deg latitudinal belt between 50N and 50S.

The satellite-observed temperatures in the "window" channel are averaged separately for day and for night for the period 12 July through 10 September 1961.

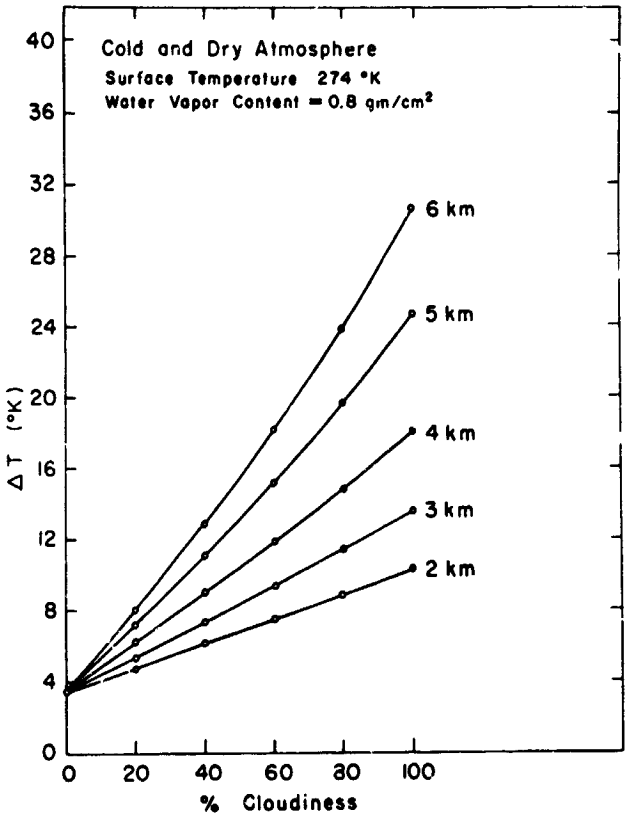

FIGURE 4.—Same as Figure 3—a case of cold and dry atmosphere.

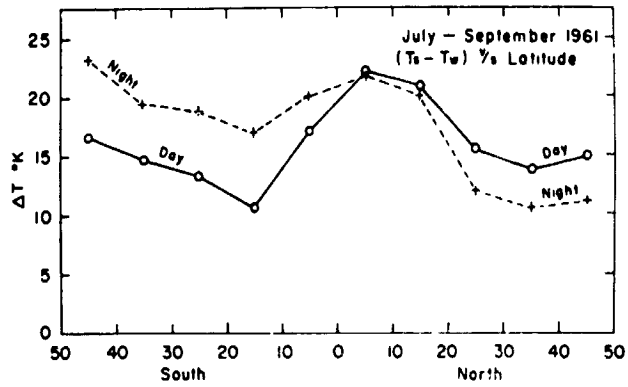

FIGURE 5.—ΔT as a function of latitude—for day and for night.

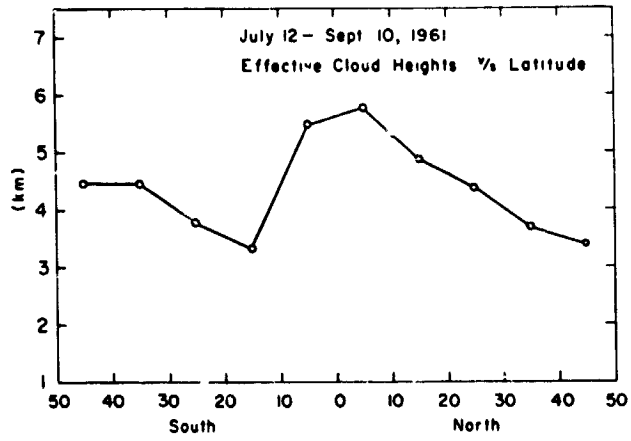

FIGURE 6.—Effective cloud top heights deduced from the daytime observation of Tiros III as a function of latitude.

The latitudinal means of day and night surface temperatures for the same period were determined from the *Monthly Climatic Data of the World* (U. S. Weather Bureau); supplementing these data were climatological estimates of Haurwitz and Austin (1944) for the oceanic regions.

The difference (ΔT) between the mean surface temperatures and the average effective temperatures measured by the TIROS channel 2 in each latitudinal belt is plotted in Fig. 5 separately for day and for night.

Latitudinal averages of daytime percentage cloud cover for the same period given by Arking are shown in Fig. 7 (Curve 1).

Now with both the ΔT and percentage cloud cover being known for daytime, we can use our nomograms (e.g., Figs. 3 and 4) to determine the average daytime cloud height for each latitudinal belt. The heights thus deduced are plotted as a function of latitude in Fig. 6.

If we assume that, on an average, cloud heights derived from the daytime measurements are also valid for the night, we can now use the ΔT values for the night (Fig. 5) and the heights plotted in Fig. 6 to determine the nighttime cloud cover as a function of latitude.

The resulting latitudinal distribution of the nighttime cloud cover is plotted as Curve 2 in Fig. 7.

A comparison of the day and night curves immediately shows that in the Southern Hemisphere, which is largely oceanic, the percentage cloudiness is much higher at night than during the day. In the Northern Hemisphere, on the other hand, the nocturnal cloud cover could be as low as ~20 percent for the latitudes of 20 to 40 deg.

These results are based on the debatable assumption that, on an average, for a given latitudinal belt the cloud-top heights do not change from day to night. In case this assumption is not correct, our results would then indicate that,

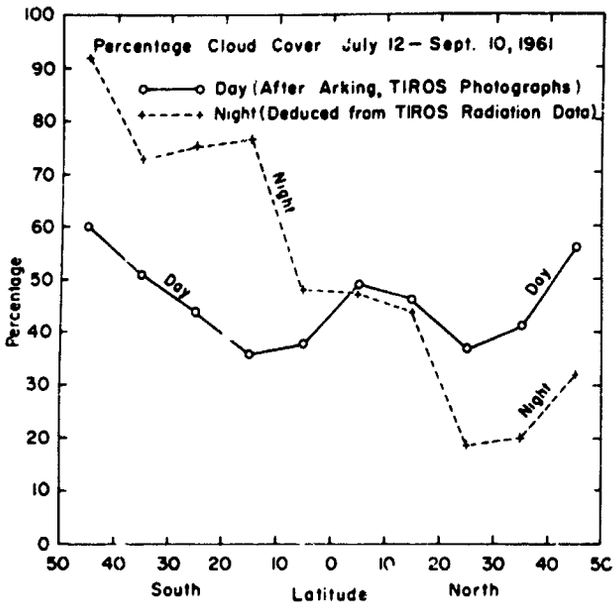

FIGURE 7.—Curve 1. Daytime average percentage cloud cover for the period 12 July through 10 September as a function of latitude (after Arking). Curve 2. Nighttime average percentage cloud cover for the same period deduced from Tiros window channel data.

in order to have the same amount of cloudiness for both day and night, the cloud heights in the Southern Hemisphere should be 2 to 4 km higher at night than in the daytime, and lower by 1 to 3 km in the Northern Hemisphere.

Similar analysis of the TIROS radiation data can also be made to determine the longitudinal as well as latitudinal distribution of nighttime cloud cover, but it requires more detailed information on the global distribution of surface temperatures, water vapor, and variations in the emissivities of land areas (Beuttner and Kern, 1963).

ACKNOWLEDGMENT

I wish to thank Professor R. M. Goody for reading over the manuscript and making valuable comments, L. Umscheid for programming and computing on an IBM 7094 and A. Liebman for his valuable assistance during the preparation of this paper.

REFERENCES

ARKING, A., 1964: The latitudinal distribution of cloud cover from TIROS photographs. *Science*, **143**, 569–572.

BANDEEN, W. R., R. A. HANEL, J. LICHT, R. A. STAMPFL and W. G. STROUD, 1961: Infrared and reflected solar radiation measurements from the TIROS II meteorological satellite. *J. Geophys. Res.*, **66**, 3169–3185.

BEUTTNER, K. J. K., and C. D. KERN, 1963: Infrared emissivity of the Sahara from TIROS data. *Science*, **142**, 671–672.

DAVIS, P., 1962: A re-examination of the heat budget of the troposphere and lower stratosphere. *Scientific Report No. 3*, Contract No. AF 19(604)-6146, Research Division, College of Engineering, New York University.

HAURWITZ, B., and J. M. AUSTIN, 1944: *Climatology*. New York, McGraw-Hill Book Co., Inc., 410 pp.

LONDON, J., 1957: A study of the atmospheric heat balance. Final Report, Contract No. AF 19(122)–165, Research Division College of Engineering, New York University.

NORDBERG, W., W. R. BANDEEN, B. J. CONRATH, V. KUNDE and I. PERSANO, 1962: Preliminary results of radiation measurements from the TIROS III meteorological satellite. *J. Atmos. Sci.*, **19**, 20–30.

PRABHAKARA, C., and S. I. RASOOL, 1963: Evaluation of TIROS infrared data. *Proc. First Internat. Symposium on Rocket and Satellite Meteor.*, Amsterdam, North-Holland Publishing Co., 234–246.

SHIFFRIN, K. S., 1961: Spectral properties of clouds. *Geofis. pura. appl.*, **48**, 129–137.

WARK, D. Q., G. YAMAMOTO and J. H. LIENESCH, 1962: Methods of estimating infrared flux and surface temperature from meteorological satellities. *J. Atmos. Sci.*, **19** 369-384.

N64-24[illegible]

GLOBAL DISTRIBUTION OF THE NET ENERGY BALANCE OF THE ATMOSPHERE FROM TIROS RADIATION DATA*

S. I. RASOOL†

The radiation data from Tiros II and Tiros III have been analyzed to obtain the monthly averages of the global distribution of the total outgoing radiation from the earth. These data have been combined with climatological estimates of the incoming radiation for the same periods to obtain monthly averages of the regional distribution of the net energy balance. The results show that these data could be useful in studies of the meridional circulation and the evolution of large-scale weather systems.

We have carried out an analysis of the radiation data acquired by the Tiros meterorological satellities, in order to determine the regional and time variations in the energy balance of the earth and its atmosphere.

The energy balance of the earth-atmosphere system is made up of the difference between the incoming solar radiation, mostly in the visible, and the outgoing terrestrial radiation in the infrared. It is well known that the latitudinal variation of the energy balance shows an excess of incoming solar radiation over outgoing radiation near the equator, and a deficiency at the poles. It is this variation of the energy balance with latitude that drives the atmospheric heat engine. Thus, through the determination of the latitudinal average of the energy balance with the aid of the Tiros data, we obtain the information which is necessary to understand the general circulation of the atmosphere.

At the same time, we have obtained some information regarding the regional variations in the energy balance of the earth-atmosphere system. Knowledge of these variations gives us a very important source of information for the understanding of large-scale weather systems.

Simpson (*1*) carried out the first extensive studies of the atmospheric energy balance, by the application of a simplified radiation theory to empirical physical models of the atmosphere. This problem has since been re-examined by Houghton (*2*), London (*3*), Budyko (*4*), and others.

The radiation instrumentation in Tiros, and the physical significance of this experiment, have already been discussed in detail by Bandeen *et al.* (*5*) and Nordberg *et al.* (*6*).

Three of the five channels of the Tiros radiometer measure terrestrial radiation in the far infrared, corresponding to wavelength intervals of 5.8 to 6.5 μ, 7 to 13 μ, and 7 to 30 μ. The other two channels record the solar radiation reflected by the earth, in the visible spectrum, which gives an estimate of the albedo of any region.

In Tiros II and Tiros III, which were active for 5 and 3 months, respectively, the channels which measure the reflected visible energy degraded very quickly, and almost no data are available for these channels. It is also possible to obtain information regarding the solar input by the statistical analysis of the Tiros cloud-cover photographs (*7*), but this analysis is still in a preliminary stage. Therefore, for this first study of the energy balance, we have used the climatological estimates of Budyko (*4*) for the incoming radiation. These give the monthly averages of solar radiation reaching the ground as a function of latitude and longitude, as derived from ground-based pyrohelimeter data.

For the outgoing radiation we have used the Tiros data in the infrared channels. Channel 4, which is sensitive in the 7- to 30-μ interval, and thus records almost 80 percent of the total outgoing radiation from the earth, also degraded after approximately 1 month in each of the

*Published in *Science*, 143(3606):567-569, February 7, 1964.

†Goddard Space Flight Center and New York University, New York.

satellites. The data from channel 2, sensitive in the 7- to 13-μ interval, however, is available from 23 November 1960 to 12 April 1961 for Tiros II and from 12 July to 10 September 1961 for Tiros III. There was some degradation in this case also, but fairly good estimates of the correction factors for this channel are now available.

Wark *et al.* (*8*) have shown that data from this channel can be used to obtain reasonably good estimates of the total outgoing radiation from the earth. Numerical factors for converting channel 2 measurements to total outgoing radiation are now available for both Tiros II and III. A comparison between the values of total outgoing radiation derived from channels 4 and 2 for the overlapping period give satisfactory results.

To obtain an estimate of the temporal as well as regional variations in the total outgoing flux, we have divided the surface of the earth into intervals of 10° latitude by 10° longitude between 50°N and 50°S. Because the inclination of the satellite orbit is 48° the data for polar regions are not available. All measurements made by the satellite in each of these intervals, at nadir angles less than 25°, have been converted to the total outgoing flux and averaged separately for each month. There are approximately 500 observation points per month in each 10° square.

The total outgoing flux estimated in this manner is, however, liable to have a small diurnal bias. This is because the orbit of the satellite precesses in right ascension at a rate of 6° per day, or it has a precession period of 9 weeks. Therefore our results for the total outgoing radiation are affected by the diurnal variation of the ground temperature. However, this effect is small for the particular case of this study which is concerned with the long-period averages over large areas. Because of the cloudiness and the presence of water vapor, the average of the channel-2 data over large regions and extended periods of time does not give the ground temperature, but has been shown (*9*) to give the effective temperature at a height of about 3 km, and therefore the effect of the diurnal variation is much reduced.

As mentioned earlier, for the incoming radiation we have used the climatological estimates of Budyko (*4*), which are based on the ground observations of solar radiation, and are given as monthly averages, also in 10° by 10° grids. These values were corrected for the absorption of solar radiation by the atmosphere, which, according to London (*3*), varies with latitude and season and is about 30 to 40 percent of the radiation which reaches the ground. The energy balance for each 10° by 10° grid, that is, the difference between these corrected values of incoming energy and the Tiros-measured values of the outgoing energy, is plotted on a month by month basis in Figs. 1 through 6.

These correspond to the months of December 1960 and January, February, March, July, and August 1961, respectively. The dark areas correspond to a positive energy balance, that is, an excess of incoming radiation over the outgoing. The light areas indicate regions of negative balance. In these figures, the darkest shade (for example, southwestern United States in July) has a value of $>+1.75\times10^5$ ergs cm^{-2} sec^{-1}, while the lightest shade (for example, 40°N to 50°N belt in December) corresponds to $<-1.65\times10^5$ ergs cm^{-2} sec^{-1}. The intermediate values of the energy balance are plotted, in steps of about 0.5×10^5 ergs cm^{-2} sec^{-1}, as seven gradations of the shading level.

The two triangular regions comprising parts of South America and Siberia have been left blank because data from Tiros are not available in those regions. Also the several other 10° by 10° grids left blank in March and July are due to nonavailability of data from Tiros for these regions.

A preliminary examination of these figures reveals several interesting features.

1) In December and January, the regions of maximum positive energy input are located in the latitudinal belt of 20°S to 50°S, while in July and August it is the 10°N to 40°N belt which has a high excess of energy. The evolution of this phenomenon is revealed by the charts for February and March.

2) The geographical distribution of the energy balance appears to be such that the desert areas of Africa, Australia, the Middle East, and southwestern United States show extreme positive energy inputs in the local summer.

3) The effect of the monsoon over India is noticeable in comparing the charts for March and August 1961. The net energy input over India is lower in August than in March, presumably

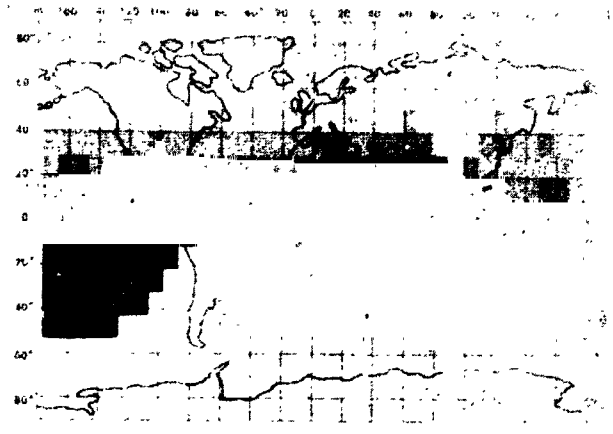

FIGURE 1.—December 1960

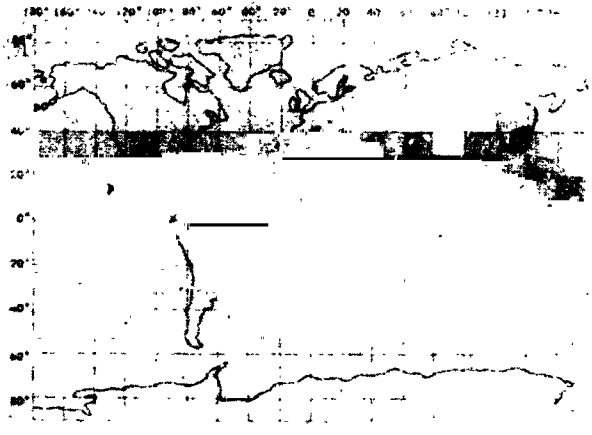

FIGURE 2.—January 1961

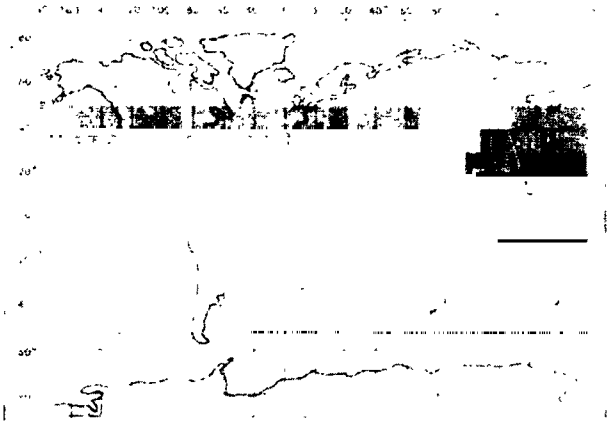

FIGURE 3.—February 1961

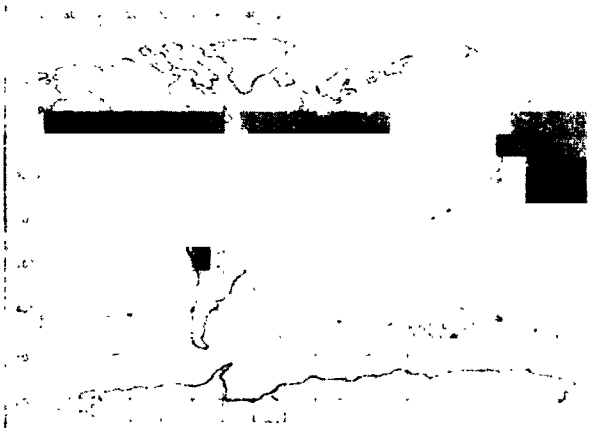

FIGURE 4.—March 1961

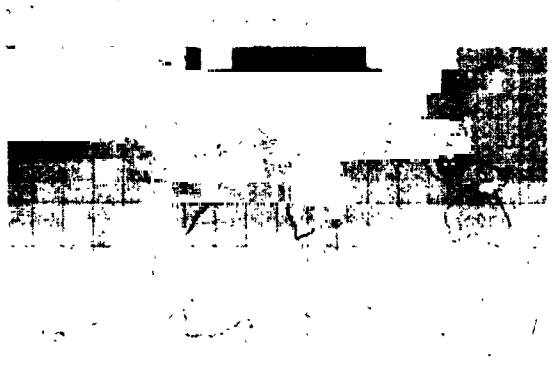

FIGURE 5.—July 1961

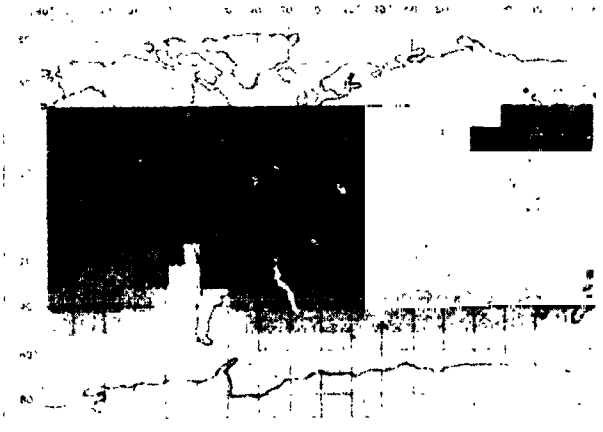

FIGURE 6.—August 1961

FIGURES 1–6.—Distribution of net energy balances for the months of December 1960 (Figure 1), January 1961 (Figure 2), February 1961 (Figure 3), March 1961 (Figure 4), July 1961 (Figure 5), and August 1961 (Figure 6). Extreme dark shade $\sim > +1.75 \times 10^5$ ergs cm^{-2} sec^{-1} and extreme light shade $< = 1.65 \times 10^5$ ergs cm^{-2} sec^{-1}.

because of the heavy monsoon cloud cover, although if it were not for the monsoon, one would expect a very high excess of energy in the summer month of August.

4) In the Northern Hemisphere, the region of the western Pacific appears to show a relative deficit in energy during all the 6 months. This area is well known for strong cyclogenic activity.

As in the case of the monsoon, the high cloudiness produced by the cyclogenesis probably accounts for the observed low input in energy.

A detailed analysis of these charts, in conjunction with the actually observed global distribution of the weather patterns for the respective months, may provide a better understanding of the role played by the energy balance of the atmosphere in the evolution of weather systems.

REFERENCES AND NOTES

1. G. C. Simpson, *Mem. Roy. Meteorol. Soc.* **3**, No. 23, 53 (1929).
2. G. H. Houghton, *J. Meteorol.* **11**, (1954).
3. J. London, "A study of the atmospheric heat balance," *Final Report*, Contract No. AF 19 (122)-165, Research Division, College of Engineering, New York University, New York, 1957.
4. F. A. Budyko, Jr., *The Heat Balance of the Earth's Surface*. Translated from the Russian edition by Nina A. Stepanova (U.S. Weather Bureau, Washington, D.C., 1958).
5. W. R. Bandeen, R. A. Hanel, J. Licht, R. A. Stampfl, W. G. Stroud, *J. Geophys. Res.* **65**, 3165 (1961).
6. W. Nordberg, W. R. Bandeen, B. J. Conrath, V. Kinde, I. Persano, *J. Atm. Sci.* **19**, 20 (1962).
7. A. Arking, *Science*, this issue.
8. D. G. Wark, G. Yamamoto, J. H. Lienesch, "Methods of estimating infrared flux and surface temperature from meteorological satellites," *J. Atmospheric Sci.* **19**, 369 (1962).
9. C. Prabhakara and S. I. Rasool, in *Proceedings of the 1st International Symposium on Rocket and Satellite Meteorology*, H. Wexler and J. E. Caskey, Jr., Eds. (North-Holland, Amsterdam, 1963).

10. I thank J. London, R. M. Goody, J. Charney, and R. Jastrow for many illuminating discussions, and Conrad Hipkins who computed and plotted these data on an IBM 7094 and SC 4020.

INTENSITIES OF 9.4μ AND 10.4μ CO_2 BANDS*

S. I. RASOOL

The intensities of the 9.4 μ and 10.4 μ CO_2 bands have been computed theoretically using, as the basis of our calculations, the line profiles at the centers of these bands published by Migeotte, Neven, and Swensson (1957). The band intensity values thus obtained are as follows:

9.4 μ band -0.0180 cm^{-2}-$atm.^{-1}$ at 265°K

10.4 μ band -0.0098 cm^{-2}-$atm.^{-1}$ at 265°K

The ratio of the two band intensities is 1.84 which is closer to the value of 1.7 given by Kostkowski (1955) than to 2.4 reported by Penner (1959).

The 9.4 μ and 10.4 μ CO_2 bands are extremely weak, and for the amount of CO_2 present in the earth's atmosphere ($\sim$0.03 percent) they do not play any significant role in the radiation processes within the terrestrial atmosphere. For this reason theoretical and experimental investigations of these bands have been rather limited. Also the two results available in the literature (Penner, 1959 and Kostkowski, 1955) differ rather significantly from each other.

For the purposes of studying radiative properties of the atmospheres of the other planets, Venus and Mars for example, where the amount of CO_2 in the atmosphere may be greater than in the earth's by several orders of magnitude, these bands do become important (Jastrow and Rasool, 1963). Therefore, in the absence of generally accepted values of the intensities of 9.4μ and 10.4μ bands, we have attempted to estimate them independently.

The method used is as follows: The solar infrared spectrum published by Migeotte *et al.* (1957) contains many lines at the center of the 9.4 μ and 10.4 μ bands due to absorption by CO_2 present in the earth's atmosphere. Measuring the total absorption within these lines and applying the Ladenburg and Reiche (1911) solution we calculate the intensities of lines in the P and R branches of the bands. The half width of the lines was assumed to be 0.09 cm^{-1} at NTP, and the amount of CO_2 in the absorption path was determined on the assumption that the total CO_2 in the earth's atmosphere is 2.40 m-atm. These line intensity values were then used to obtain a mean value of the band intensity using the classical relation (see, for example, Goody, 1963).

Internal consistency in the band intensity calculations was achieved when the effective temperature of the atmosphere above Jungfraujoch observing station was assumed to be 265°K. This is $\sim$6°K lower than the recorded surface temperatures during these observations.

In the following table we give the band intensity values determined by the method mentioned and values give by the other authors.

Intensities in cm^{-2}-atm^{-1} of CO_2 *Bands at* 9.4 μ *and* 10.4 μ

	9.4 μ (S′)	10.4 μ (S″)	T	S′/S″
This work	0.0180	0.0098	265°K	1.8
Kostkowski (1955)	0.0465	0.0281	329°K	1.7
Penner (1959)	0.0532	0.0219	297°K	2.4

The band intensity values given by Kostkowski, when reduced to 265°K, compare fairly well with our results, but those of Penner, especially of the 9.4 μ band, are significantly higher than ours.

I wish to thank Professor R. M. Goody of Harvard University for suggesting this method of calculation.

REFERENCES

R. M. Goody, *Atmospheric Radiation*, Cambridge Univ. Press, Cambridge, 1963.

R. Jastrow and S. I. Rasool, "Radiative transfer in the atmospheres of Venus and Mars," in *Space Research III*, ed. W. Priester, North Holland Publ. Co., 1963.

H. J. Kostkowski, Dissertation, the John Hopkins Univ., 1955.

R. Ladenburg and R. Reiche, *Annalen der Physik*, **421**, 181, 1911.

M. Migeotte, L. Neven and J. Swensson, The solar spectrum from 2.8 μ to 23.7 μ. *Mém. Soc. Roy. Sc., Liège*, 1957.

S. S. Penner, *Quantitative Molecular Spectroscopy and Gas Emissivity*. Addisor Wesley, Mass. 587 pp., 1959.

*Published in Mémoires Soc. R. Sc. Liége, Cinquième Série, Tome IX, Extract pages 55–57.